USING 3-D SEISMIC INVERSION DATA AS A TOOL FOR PREDICTING POROSITY IN THE WILBURTON GAS FIELD, ARKOMA BASIN, SOUTHEASTERN OKLAHOMA

by

JEFFREY CHARLES FUCHS

IBRAHIM ÇEMEN, COMMITTEE CHAIR

ANDREW GOODLIFFE
DELORES ROBINSON
ROD GERTSON

A THESIS

Submitted in partial fulfillment of the requirements
for the degree of Master of Science
in the Department of Geological Sciences
in the Graduate School of
The University of Alabama

TUSCALOOSA, ALABAMA

2012

ABSTRACT

Understanding and identifying changes in rock properties over an area is critical in characterizing a reservoir. In order to identify porosity changes, a 3-D seismic inversion volume was inverted for acoustic impedance in the Red Oak and Brazil Sandstones in the Wilburton gas field located in the Arkoma Basin, southeastern Oklahoma. The tops and bases of these two sandstones were identified to be analyzed based on acoustic impedance and porosity. Establishing a relationship between acoustic impedance and porosity allows porosity to be predicted away from the wellbore using the seismic acoustic impedance data.

Interpretation of the seismic inversion data suggests that a) there is a linear correlation between acoustic impedance and porosity in the sandstone portions of the Red Oak and Brazil Sandstones; b) seismic thickness cannot be used to predict actual thickness of these sandstone units due to variations in velocity; and c) prediction of porosity using seismic inversion data inverted for acoustic impedance in sandstone containing interbeds of shale is not reliable, and the method should be limited to homogeneous sandstone.

LIST OF ABBREVIATIONS AND SYMBOLS

1-D	One dimensional
2-D	Two dimensional
3-D	Three dimensional
AI	Acoustic impedance
API	American Petroleum Institute Units
DT	Sonic
ft	Feet
ft/s	Feet per second
g	Gram
gft/cm^3s	Gram foot per centimeter cubed second
GR	Gamma ray
Hz	Hertz
ILD	Resistivity
kg	Kilogram
kg/m^2s	Kilogram per meter squared second
km	Kilometer
LAD	Lower Atokan Detachment
LFM	Low frequency model
m	Meter
Ma	Millions of years before present

MS	Master of Science
ms	Millisecond
m/s	Meters per second
µs/ft	Microseconds per foot
OSU	Oklahoma State University
PORZ	Porosity
PSTM	Pre-stack time migrated
s	Second
SS	Sandstone
tcf	Trillion cubic feet
TWT	Two way travel time
WGF	Wilburton Gas Field

ACKNOWLEDGMENTS

I would first like to extend a special thanks to my advisor, Dr. Ibrahim Çemen, for allowing me the opportunity to work on this project. It has been a great learning experience and has provided me with a skill set that I will continue to use in my career as a professional geologist. Dr. Cemen's extensive knowledge of the Arkoma basin has been invaluable in the completion of this thesis.

I would like to thank each member of my committee for their contributions to my thesis. Dr. Andrew Goodliffe has been a great source of information on the processing of seismic data. Dr. Delores Robinson has helped me greatly with her knowledge of structural and petroleum geology. Rod Gertson has contributed to my work immensely with his geophysical expertise.

I would like to thank the companies that contributed to the completion of my thesis. Devon Energy provided the seismic and well log data that were utilized for this project. IHS has generously given The University of Alabama Department of Geological Sciences access to their software programs Kingdom Suite and Petra. Both software packages were essential in the interpretation of the seismic and well log data. Their technical support was also very helpful, and played an essential role in the completion of this thesis.

I would also like to thank Gorka Garcia of Schlumberger who was very helpful in answering specific questions about the inversion, and helped me understand the data.

Last but certainly not least, I would like to thank my friends and family. My friends provided me with balance during this challenge that helped me more than they will ever know.

My family is my foundation. I cannot thank them enough. They taught me the value of hard work and have always been there for me. Without their love, encouragement, and support none of this would have been possible.

Again I would like to thank all the people and organizations who sacrificed their time and resources to make this thesis possible. I appreciate the guidance and support all of you have given me during this process. I could not have done it without you. Thank you.

CONTENTS

LIST OF FIGURES

CHAPTER 1

INTRODUCTION

The Arkoma Basin, formed as a foreland basin during the Ouachita Orogeny in the Late Paleozoic, is located in southeastern Oklahoma and western Arkansas. It is approximately 250 miles long and 50 miles wide, and is characterized by gradual folds and minor faults (e.g., Mehdi, 1997). Collision of the North American plate and a southern landmass known as Llanoria formed the Arkoma Basin and the Ouachita Mountains during the Ouachita Orogeny (e.g., Houseknecht and Kacena, 1983). In peripheral foreland basins such as the Arkoma, sediment accommodation is attributed to flexural subsidence driven by the topographic load of the thrust belt, sediment loads in the foreland basin, and subduction loads (DeCelles and Giles,1996). The Ouachita fold thrust belt may join the Appalachian Mountains in Alabama and the Marathon fold-thrust belt in south Texas, but the nature of this connection is controversial (Figure 1) (Robinson et al., 2012).

Foreland basins, such as the Arkoma Basin are extensively studied because of their oil and gas potential. Natural gas was first discovered in the Arkoma Basin in 1902 in Sebastian County, Arkansas, but extensive drilling did not begin until deeper sands were reached in the 1960's (e.g., Branan, 1968). Modern exploration in the basin began in the 1980's. The southern portion of the basin contains several pay zones ranging from the Lower Morrowan Wapanucka Limestone to the Middle Desmoinesian McAlester Formation.

Between 2007 and 2009 three Master of Science (MS) theses were completed at Oklahoma State University (OSU) using a 3-D seismic survey from a project supported by Devon Energy. Parker (2007) delineated the structural evolution of Pennsylvanian thrusting in the western Arkoma Basin. Sadeqi (2007) constructed and balanced seven structural cross sections to determine the amount of shortening in the Spiro Sandstone. The 3-D conventional data set used by Parker (2007) and Sadeqi (2007) was later inverted for acoustic impedance. Hager (2009) interpreted stratigraphic and lithologic variations in the Spiro/Wapanucka package, and also established a relationship between acoustic impedance and porosity in the Lower Pennsylvanian Spiro Sandstone.

The main objective of this study is to determine if a relationship between acoustic impedance and porosity exists in the Middle Atokan Brazil and Red Oak Sandstones. These sandstones have greater fluctuations in thickness than the Spiro Sandstone, and are interbedded with shale. Large acoustic impedance contrasts are present at the top and base of the rock units, facilitating horizon interpretation. Establishing a relationship between acoustic impedance and porosity allows seismic inversion data to be used to determine the reservoir rock properties away from the well bore.

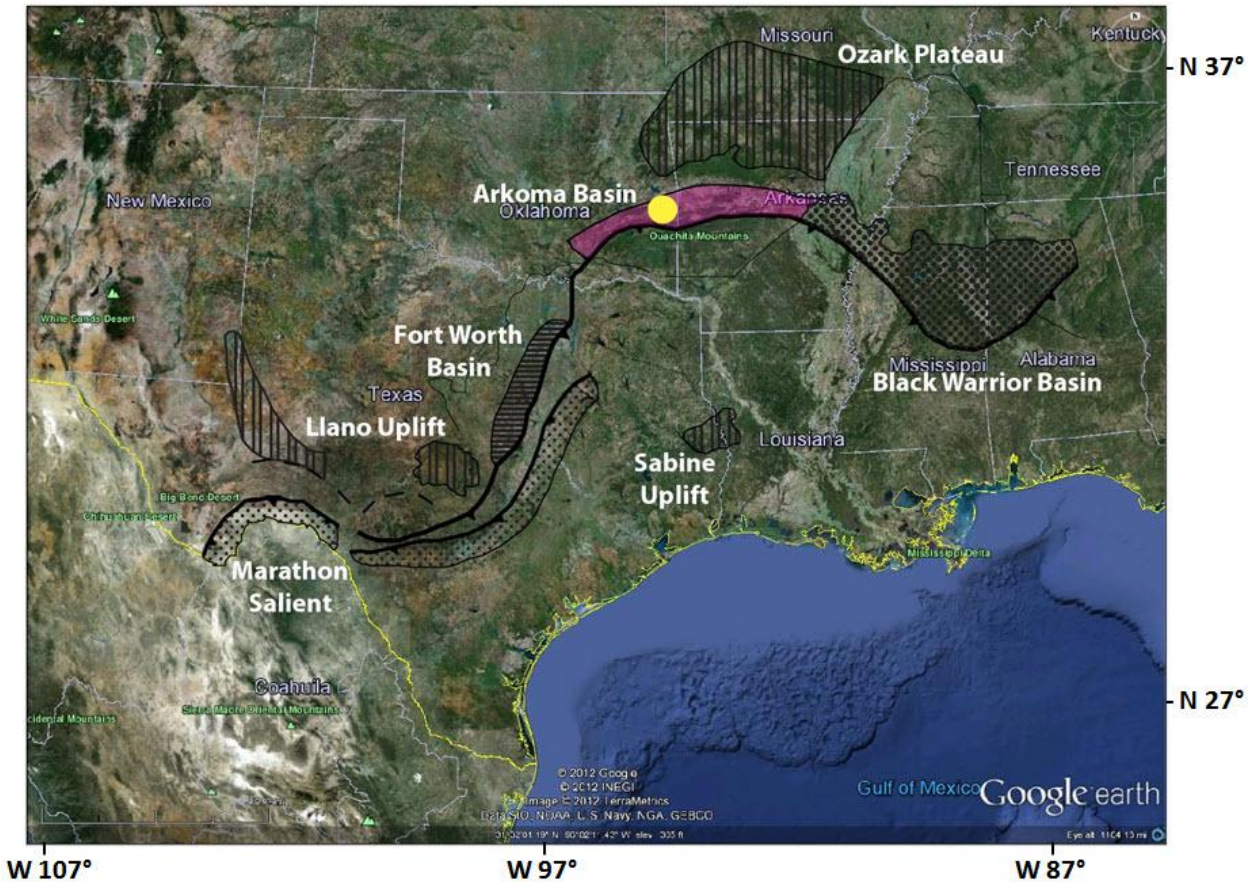

Figure 1. Yellow circle indicates approximate location of thesis study area within the Arkoma Basin (pink) along the Ouachita fold-thrust belt (modified from Çemen et al., 2001).

Study Area

The Ouachita Mountains are divided into three distinct provinces on the basis of structural and stratigraphic features. These provinces from north to south are the Frontal fold thrust belt, Central fold thrust belt, and Broken Bow uplift (Figure 2). The Arkoma Basin lies adjacent to the Frontal Belt in the north, and is separated from the Ouachita Mountains by the Choctaw Fault, which is the leading edge thrust of the Ouachita Mountains. The study area is located in the Wilburton gas field (WGF), in the transition zone between the Frontal Belt of the Ouachita Mountains and the Arkoma Basin (Figure 2). The WGF is in Latimer and Pittsburg Counties, Oklahoma, has produced over a trillion cubic feet of gas (tcf).

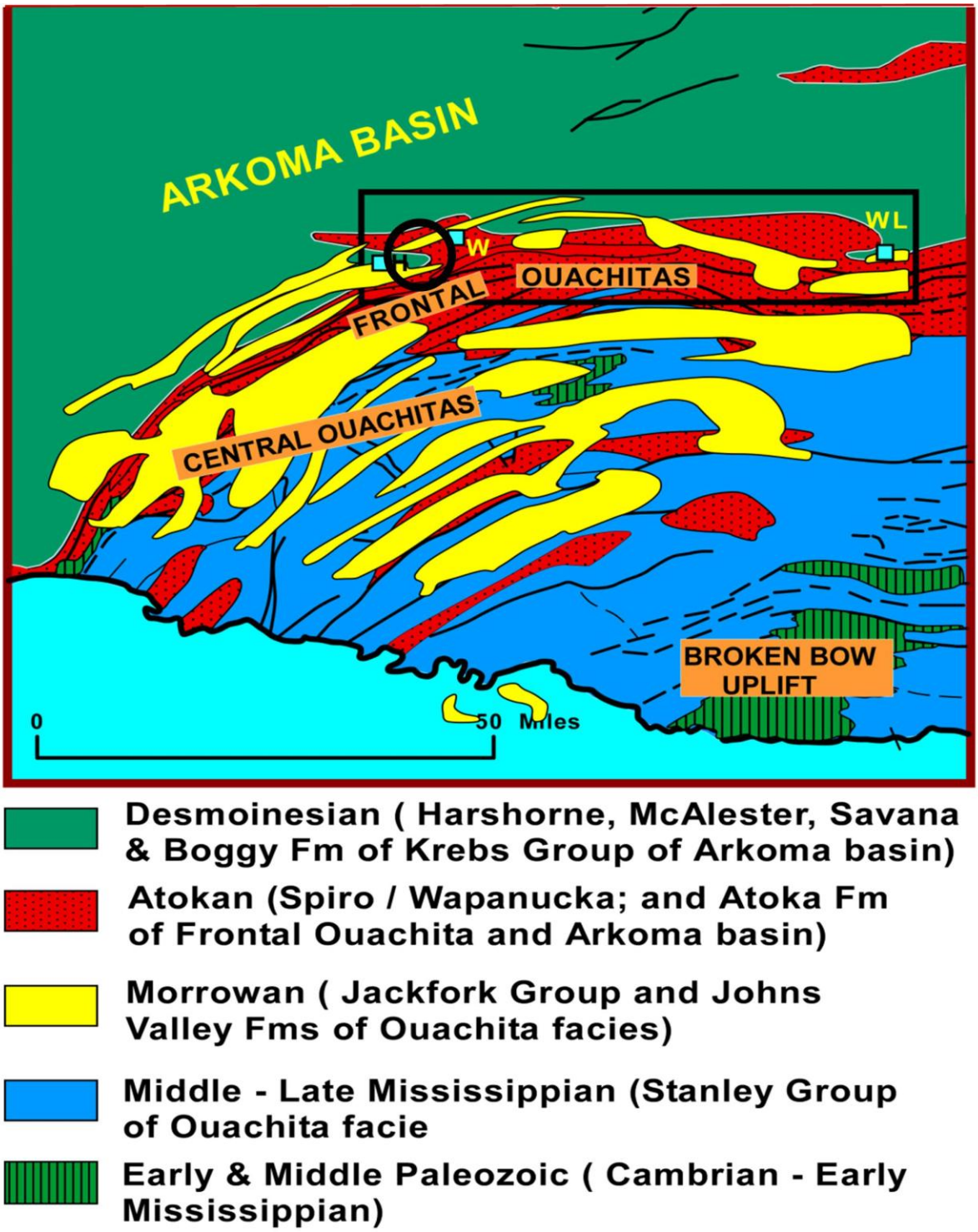

Figure 2. Study area location location (black circle) in the Arkoma Basin on the edge of the Frontal Ouachitas (black box) (Çemen et al., 2001).

Purpose of Study

The purpose of the study is to determine if acoustic impedance changes can be tied to porosity changes in the Middle Atokan Brazil and Red Oak Sandstones. If a relationship between acoustic impedance and porosity can be established, this relationship can help identify productive zones (higher porosity) in areas with sparse well control.

Secondly, this study will determine if seismic acoustic impedance can be used to map thickness changes away from the wellbore in the Brazil and Red Oak Sandstones by picking the top and base of each unit more accurately. Ultimately, using these relationships in conjunction with the inversion data will allow the interpreter to locate areas of better reservoir quality (i.e stratigraphically thicker and more porous) within the sandstones.

Methodology

In 2004, a research contract between Devon Energy and the OSU Boone Pickens School of Geology provided a 3-D seismic data set. In 2005, Odegaard America Inc. inverted the data set for acoustic impedance, making it possible to map property changes in rocks including porosity, fluid content, clay content, and cementation.

The 3-D seismic inversion data were imported into KINGDOM Suite, as well as LAS files and formation tops (64 wells). Horizons and major faults have been picked and calibrated by well control (Parker, 2007). Hager (2009) used porosities from well log data and acoustic impedance values from the inversion seismic data and cross-plotted them to derive relationships between porosity and acoustic impedance in the Spiro Sandstone. Time-depth charts were created using sonic logs. The time-depth conversion was used to convert well-based acoustic impedance data to time in order to compare it to the seismic reflection.

The following steps were used to determine if a correlation between porosity and acoustic impedance exists in the Middle Atokan Brazil and Red Oak Sandstones in the Arkoma Basin:

1) The top and base of the Brazil and Red Oak Sandstones were picked over the survey area.
2) Cross-plots of acoustic impedance versus porosity were generated for the Brazil and Red Oak Sandstones to determine if a relationship existed.
3) Seismic thickness and amplitude maps for the Brazil and Red Oak Sandstones were created using the inversion data to compare thickness and impedance changes.

CHAPTER 2

STRUCTURAL EVOLUTION OF THE ARKOMA BASIN

The Arkoma Basin extends more than 250 miles across southeastern Oklahoma into west-central Arkansas (e.g., Ronck, 1997). The northern margin of the Arkoma Basin is bounded by the Ozark Uplift that stretches through northeastern Oklahoma, and northwestern Arkansas. The eastern boundary of the basin is bounded by the Cretaceous and Tertiary cover of the Gulf Coast and Mississippi River Embayment in central Arkansas. On the surface, the southern margin of the basin is marked by the Choctaw Fault, which is the leading edge thrust for the Ouachita fold thrust belt, and is generally recognized as the boundary between the Arkoma Basin and the Ouachita Mountains.

Adjacent to the Ouachita Mountain system, the deepest part of the Arkoma Basin contains approximately 30,000 feet of Pennsylvanian and Mississippian age sediment (Branan, 1968). Multiple tectonic pulses have occurred throughout the depositional history of the region, creating a variety of structural styles (Arbenz, 1989).

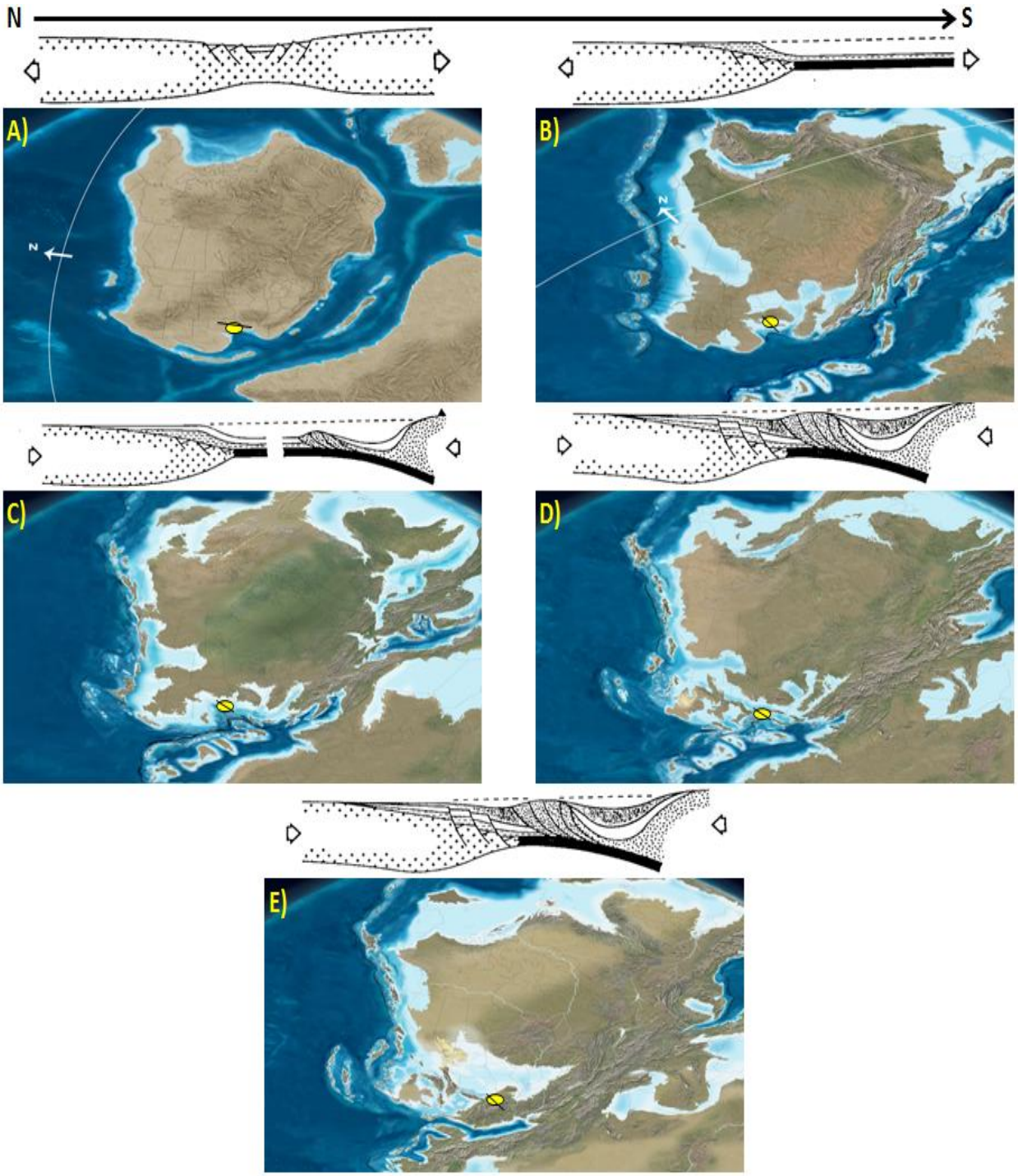

Figure 3. Paleogeographic maps showing different stages of evolution of the Arkoma Basin with structural cross sections drawn from north to south. A) Cambrian (510Ma), B) Devonian (385Ma), C) Mississippian (345Ma), D) Pennsylvanian (315Ma), E) Pennsylvanian (300 Ma) (Blakely, 2005; and Houseknecht and Kacena, 1983). Yellow circle corresponds to approximate location of thesis study area.

In Late Proterozoic or Early Paleozoic time, the Iapetus ocean basin opened (Houseknecht and McGilvery, 1990). Following initial rifting, a passive margin developed along the southern margin of North America in Late Paleozoic to Early Cambrian time (Figure 3a). Passive margin sediments were deposited through Early and Middle Paleozoic time (Figure 3b). The shelf environment, forming the Arbuckle facies through Cambrian and Devonian time, is predominantly carbonate with lesser amounts of shale and quartzose sandstone (Houseknecht, 1986). Accommodation space was created by widespread normal faulting due to loading, but subsidence and deposition occurred very slowly (Houseknecht and McGilvery, 1990). In the deeper water, the Ouachita facies comprise large volumes of deep marine shale, limestone, sandstone, and small amounts of bedded chert controlled by gravity flow processes within a starved basin (Houseknecht, 1986).

By Devonian or Early Mississippian time, the ocean to the south began to close via a southward-dipping subduction zone (Figure 3c) (Houseknecht and McGilvery, 1990). Evidence for the presence of this subduction zone and associated volcanism is found in the Mississippian Stanley Group in the form of widespread Devonian metamorphism and volcani-clastic sedimentation (Houseknecht, 1986). Nicholas and Waddell (1982) proposed that the northern edge of Llanoria had a possible magmatic arc complex. Therefore, the Ouachita Mountains could have begun as an accretionary front on the northern margin of the subduction zone in Late Devonian to Early Mississippian time.

By Early Atoka time (315 Ma), the ocean basin was closed (Figure 3d) by the advancing collisional front from the south. The subduction complex moved northward onto the southern margin of North America, and obducted along with the accretionary prism (Houseknecht and McGilvery, 1990). The North American plate experienced flexural bending and associated

normal faulting due to tectonic loading (Houseknecht, 1986). This faulting marked the end of the stable shelf environment, and offset the basement to Early Atokan strata. These southward dipping normal faults created additional accommodation space for sedimentation, and deposition in the newly forming foreland basin matched pace. This is supported by the large quantity of shale and the thickness variations across faults in the Middle Atokan shale and sandstone (Figure 4) (Houseknecht and McGilvery, 1990) referred to as the flysch facies in the Arkoma Basin (Houseknecht, 1986).

Near the end of Atokan time, the advancing compressional front altered the stress distribution in the foreland. Extensional faulting transitioned into thin-skinned thrusting within Atokan strata creating duplexes and other related structures (Houseknecht and Kacena, 1983) (Figure 3e). After Atokan time, shallow marine and fluvial sedimentation continued until the Arkoma Basin filled in Desmoinesian time (Houseknecht and Kacena, 1983). Since Desmoinesian time, the structural configuration of the Arkoma-Ouachita system has remained relatively undisturbed with the exception of a few minor thrusting and folding events (Houseknecht and Kacena, 1983).

Çemen et al. (1995) proposed a structural model for the WGF. The model includes a triangle zone underlain by a duplex in the footwall of the Choctaw Fault (Figure 5). The triangle zone is floored by the Lower Atokan Detachment (LAD) surface, bounded to the south by the Choctaw Fault, and to the north by the Carbon Fault. A deeper detachment within the Woodford Shale, the Woodford Detachment, serves as the floor thrust of the duplex, translates the Springer Shale to the north, and dies within a backthrust towards the basin (Figure 5). Thrusting in the duplex occurred in sequence, and shortening is 60% (Çemen et al., 2001).

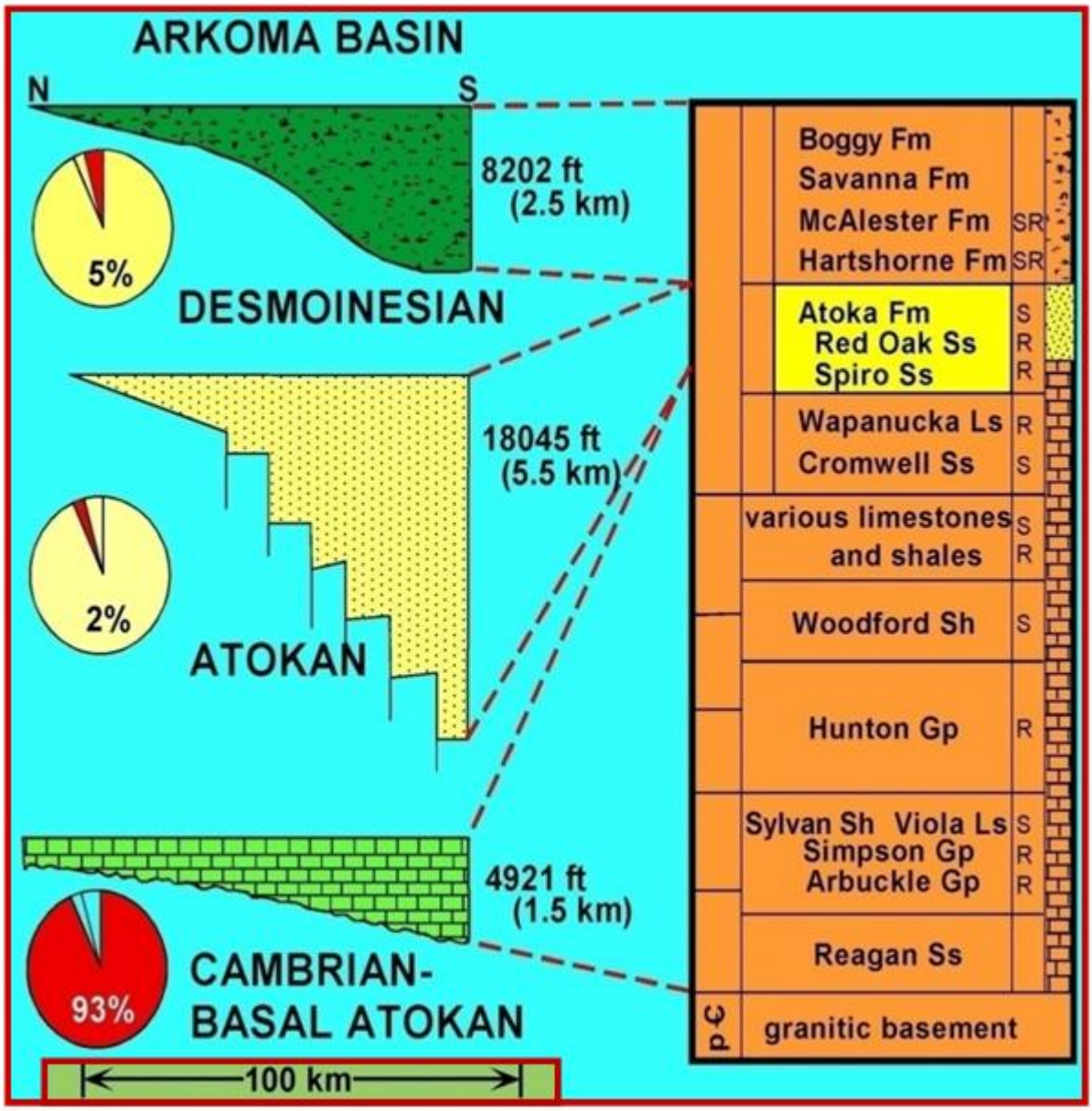

Figure 4. Stratigraphic chart and time frames illustrating the amount of deposition occurring during the evolution of the Arkoma Basin. The pie graphs illustrate the percentage of time each group of sediments were deposited in relation to the total time in which all sediments were deposited in the basin (Houseknecht, 1990).

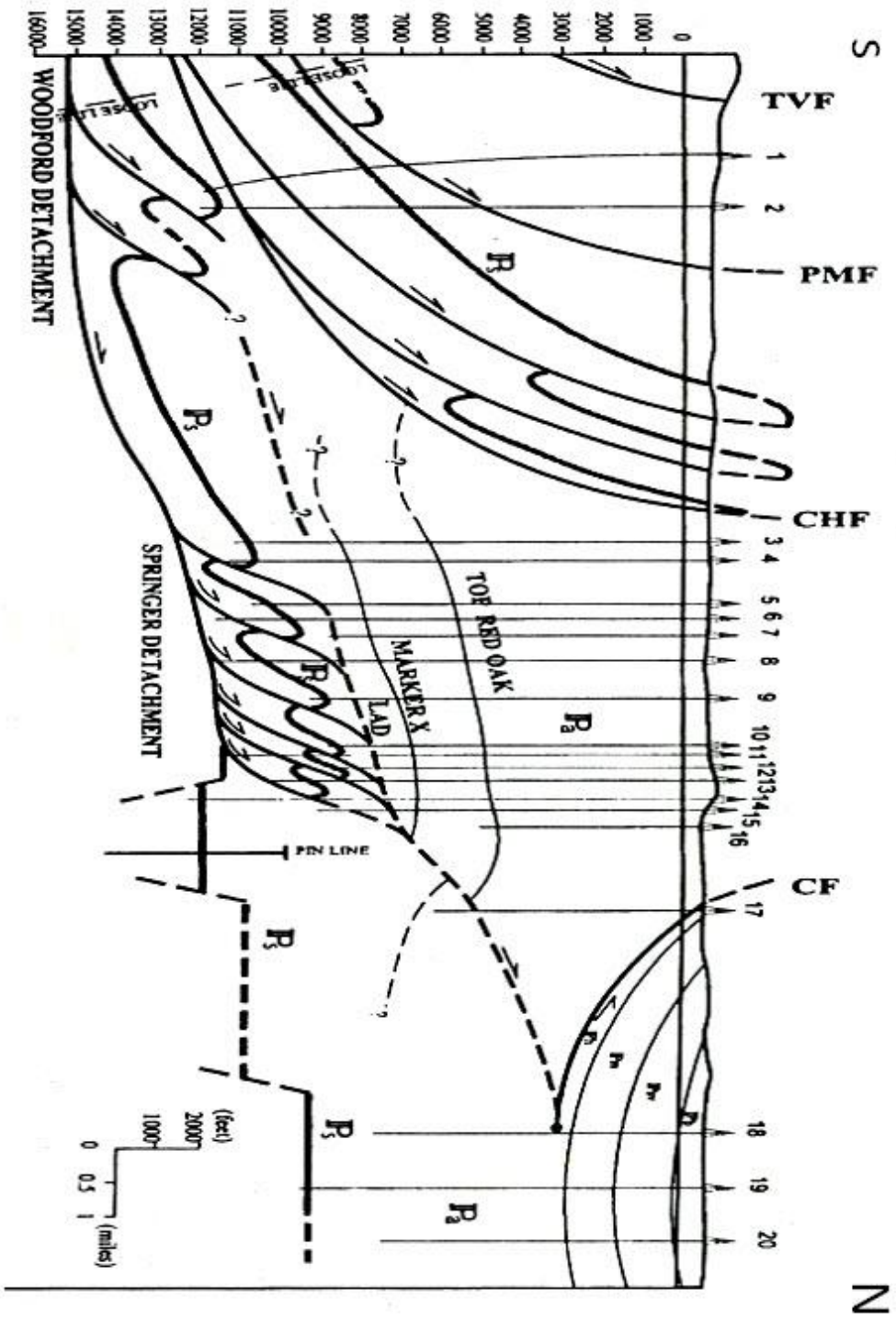

Figure 5. Wilburton gas field triangle zone interpretation (Cemen et al., 2001). CF=Carbon Fault, CHF=Choctaw Fault, PMF= Pine Mountain Fault, TVF= Ti Valley Fault and LAD=Lower Atokan Detachment

CHAPTER 3

STRATIGRAPHY OF THE ARKOMA BASIN

Both the Arkoma Basin and Ouachita Mountains have thick accumulations of sedimentary rocks spanning from Cambrian to Pennsylvanian time (Figure 6). These strata record the collapse of the deep ocean basin and development of a foreland basin through continental collision (Sutherland, 1988).

Pre-Pennsylvanian Stratigraphy

Proterozoic granite, rhyolite, and metamorphic rocks comprise the crystalline basement of eastern Oklahoma (Figure 6). The Upper Cambrian Reagan Sandstone of the Timbered Hills Group represents a time-transgressive unit deposited in all areas except topographic highs across the basement floor (Johnson, 1988). Overlying the Reagan Sandstone is the shallow, trilobite-rich Honey Creek Limestone (Ham, 1978).

The Cambro-Ordovician Arbuckle Group conformably overlies the Timbered Hills Group. The Lower Arbuckle Group is Late Cambrian in age, and composed of the Fort Sill Limestone, Royer Dolomite, and Signal Mountain Limestone. The Upper Arbuckle Group is Early Ordovician in age, and composed of the Butterfly Dolomite, McKenzie Hill, Cool Creek, Kindblade, and West Spring formations. These units represent shallow water facies. Deep-water facies of the Ouachita trough are listed in Figure 6 beside the shallow water stratigraphic equivalent.

Middle and Upper Ordovician strata are represented by shallow water carbonates of the Simpson and Viola Groups on the shelf, and deep-water shale and chert toward the basin. Limestone of the Simpson Group, in ascending order, are the Joins, Oil Creek, McLish, Tulip Creek, and Bromide formations. These represent a change toward shallower environments and are characterized by skeletal calcarenite, skeletal carbonate, mudstone, sandstone, and shale (Ham, 1978). Prominent sandstones are generally found at the base of each successive limestone. Basinal equivalents are the Blakely Sandstone and Womble Shale (Morris, 1974).

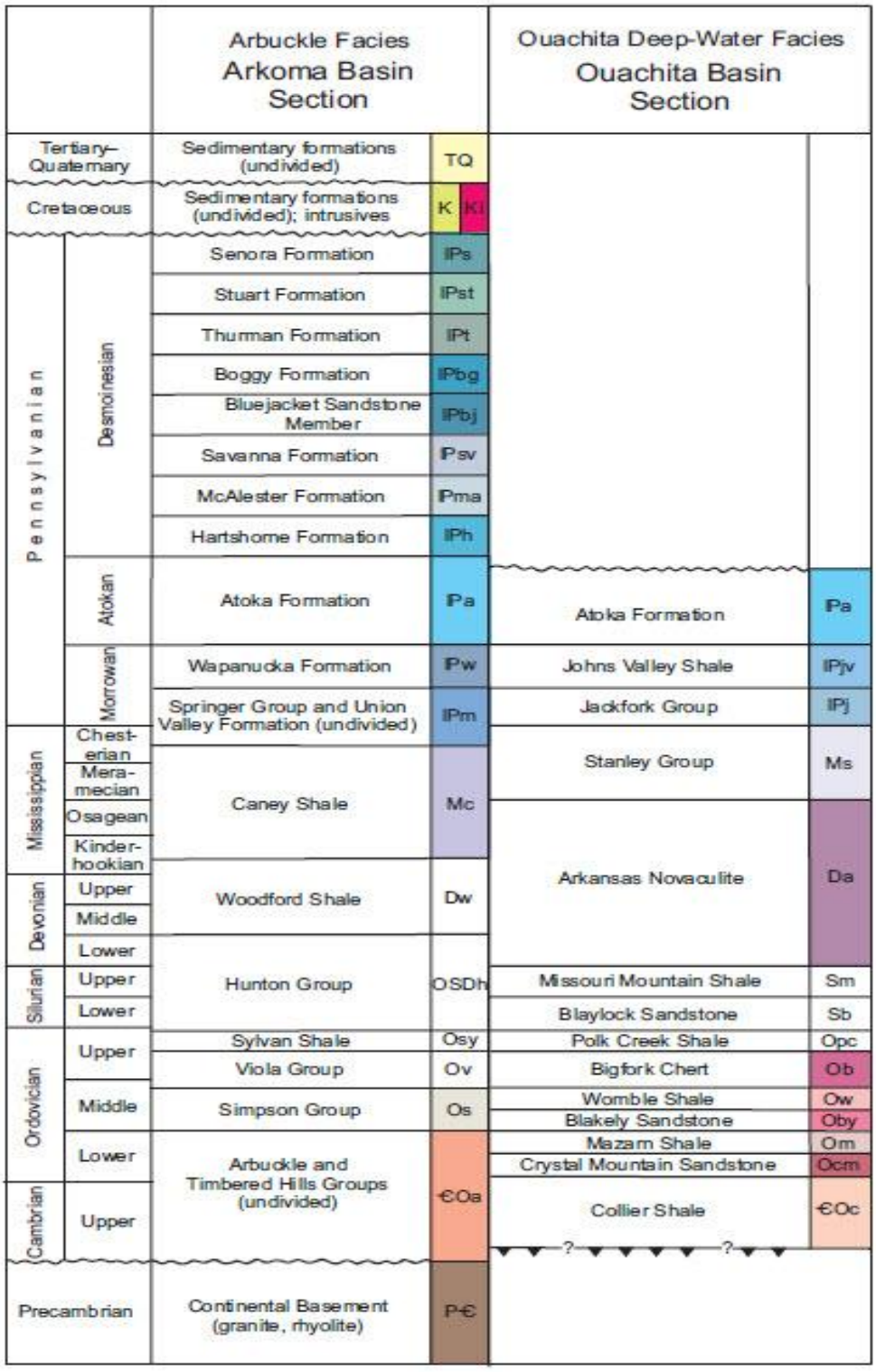

Figure 6. Stratigraphic section of the Arkoma Basin and Ouachita Mountains and correlation of Arbuckle and Ouachita facies (Suneson, 2012).

The Upper Ordovician Viola Group conformably overlies the Simpson Group. Consisting of the Viola Springs and Welling formations, these shallow carbonates display nodular chert-rich mudstone, packstone, porous grainstone, and wackestone, some of which are dolomitized (Ham, 1978). The Upper Ordovician Sylvan Shale, a green to gray shale with well-developed laminations, unconformably overlies the Viola Group.

The Ordovician to Lower Devonian Hunton Group overlies the Sylvan Shale (Ham, 1978). The Upper Devonian to Lower Mississippian Woodford Shale lies unconformably on the Hunton Group (Figure 6). This extensive source rock is predominantly dark, fissile shale, with interbedded vitreous and siliceous chert (Ham, 1978). Along the frontal Ouachitas, this stratigraphic unit represents a major basal detachment surface (Woodford Detachment) for the ensuing thrust system (Johnson, 1988).

The Mississippian Caney Shale was conformably deposited on top of the Woodford Shale. The upper stratigraphic boundary for the Caney Shale is based on the first appearance of siderite or clay-bearing ironstone beds, which represent shallower deposition. Ham (1978) assigned the Springer Shale a Late Mississippian age (Chesterian), based on the appearance of spores and pollens. Basinal equivalents of the Mississippian are the Arkansas Novaculite and the Stanley Group, which reflects a period of marked increase in subsidence rates for the trough.

Pennsylvanian Stratigraphy

Pennsylvanian deposition records the onset of thrusting within the Arkoma Basin and only rocks of the Morrowan, Atokan, and Desmoinesian series are present. Sedimentation patterns on the shelf did not change during Morrowan time, although large amounts of sand are present within individual facies (Johnson, 1988). Morrowan facies are approximately 1,000 feet thick towards the north, but thicken up to 6,000 feet to the south in the deeper parts of the basin. On the shelf, Morrowan rocks consist of the Cromwell Sandstone, Union Valley Limestone, and Wapanucka Limestone (Figure 7). These units were deposited during a series of small-scale transgressions and regressions, in which a number of discontinuous limestone and sandstone lenses were deposited between shale packages (Sutherland, 1988). In particular, the Wapanucka Limestone was deposited during a sea level regression, interrupted by minor shoreward movements of the coastline (Gross and others, 1995). It consists of thick platform carbonates to the west, but becomes thin and shaley to the east (Gross and others, 1995).

While sedimentation on the shelf shows only minor lithological and sedimentological variations, the deep basin underwent vast changes. Extensive growth faulting in the southern margin of the basin occured by Late Mississippian time (Houseknecht and Kacena, 1983). Morrowan shelf facies thicken southward where deep-water marine sediments, characterized by flysch deposition, are found. Large accumulations of sediment were primarily derived from the east and funneled along submarine canyons into the downthrown blocks, and became the Jackfork and overlying Johns Valley formations (Berry and Trumbley, 1968).

During an ensuing lowstand episode, the Atoka Formation was unconformably deposited on top of the Wapanucka Formation (Berry and Trumbley, 1968). The Atokan Formation is the thickest unit in the basin, approximately 15,000 feet thick in the deepest portions (Berry and Trumbley, 1968). It is informally divided into the Lower, Middle, and Upper Atoka (Figure 7). Shale comprises nearly 70% of the Atokan strata, which are broken by intermittent sandstone lenses deposited by fluvio-deltaic processes (Sutherland, 1988). Sediment transport on the shelf is predominantly from the north and northeast and carried west via longshore currents (Sutherland, 1988).

The basal Atoka is unconformable with the underlying Morrowan Series (Figure 7). It consists of the Spiro Sandstone underlain by the thick, sub-Spiro shale. In general, the Spiro Sandstone was deposited on a broad shelf from northern fluvial systems southward toward shallow marine environments (Gross et al., 1995). It consists of basal progradational/aggradational sandstone overlain by a retrogradational parasequence set (Gross et al., 1995). Depositional environments include tidal flats, deltaic, barrier islands, tidal channels, and shallow marine sand bars (Houseknecht and Kacena, 1983).

Middle Atokan sandstones include, in ascending order, the Shay, Cecil, Brazil, Diamond, Panola, and Red Oak (Figure 7). These sandstone intervals are interbedded with extensive shale packages throughout the basin making the tops and bases easy to delineate in the inversion data. Deltaic complexes interrupted by small-scale sea level changes are the dominant depositional setting, with off-shore sands characterized by gravity flow sedimentation at the base of submarine fans (Visher and Vedros, 1978).

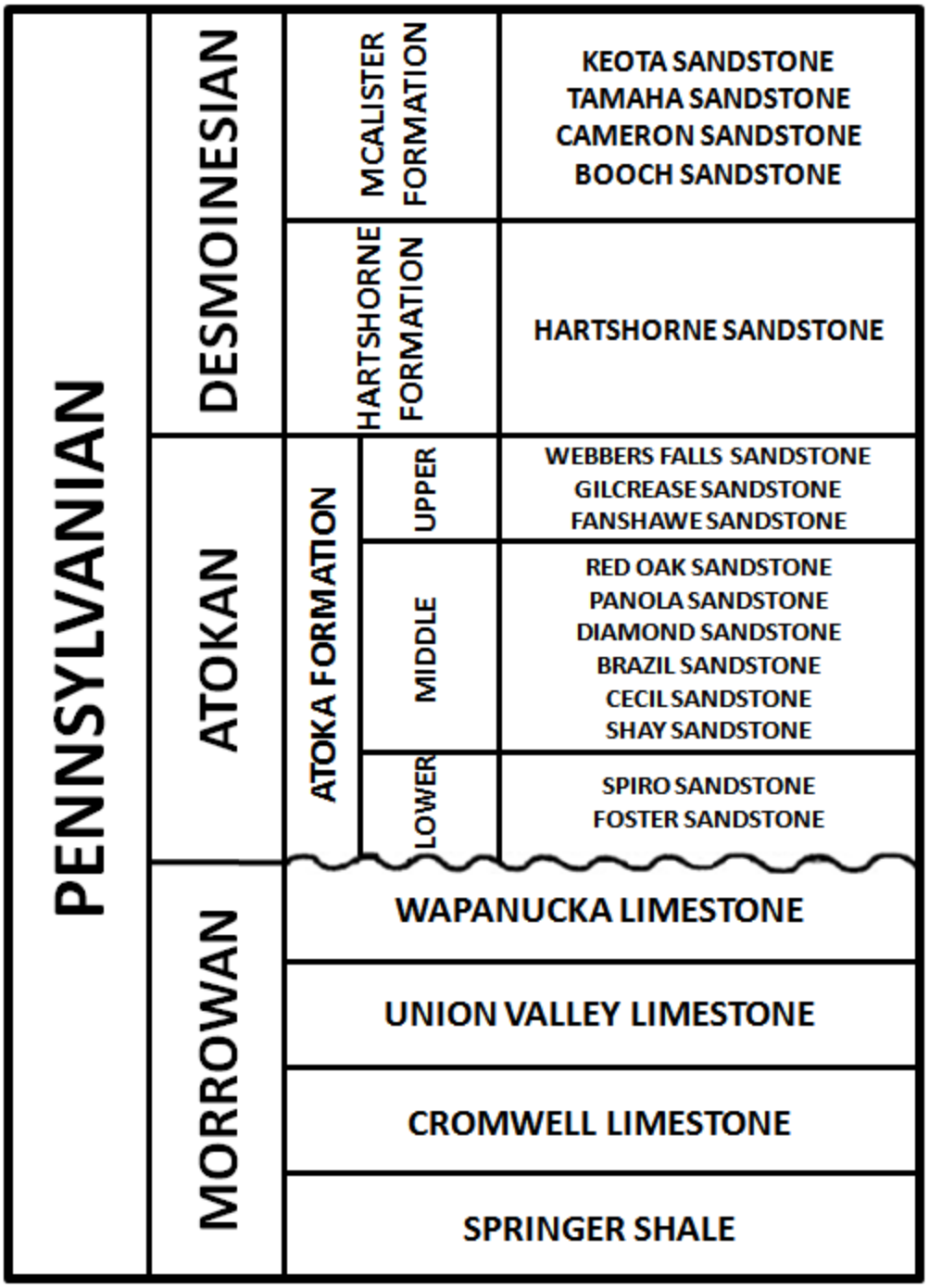

Figure 7. Detailed stratigraphic chart of the Pennsylvanian system of units within the Arkoma Basin (modified from Sutherland, 1988).

The Upper Atoka consists almost entirely of mudstones deposited within shallow shelf to deltaic environments (Sutherland, 1988). Growth faulting that dominates middle Atokan stratigraphy does not penetrate these shales, suggesting that the normal faulting induced by flexural down warping ceased by middle Atokan time.

The basin is overlain at the axis by Desmoinesian rocks comprising the Krebs, Cabaniss, and Marmaton Groups (Figure 7). Desmoinesian strata are not found in the frontal Ouachitas; thus it is unknown whether younger strata were ever deposited in the region. Northward on the shelf, the depositional environment continued to be influenced by fluvio-deltaic processes, with intermittent sandstone lenses separated by thick, shallow marine shale (Sutherland, 1988). The Krebs Group is composed of the Hartshorne, McAlester, Savanna, and Boggy formations (Figure 6).

CHAPTER 4

SEDIMENTOLOGY OF THE ATOKAN SANDSTONES

The Lower Atokan Spiro Sandstone is a fine to medium grained, well sorted, well rounded quartz arenite (Figure 8). It was deposited as a reworked barrier island deposit that was later deposited as a sheet sand (Sutherland, 1988; Sadeqi, 2007) (Figure 9). The Spiro has good lateral continuity and high net to gross sand (Gross, 1995).

The Middle Atoka interval in Oklahoma is composed predominantly of shale with a few sandstone units (Figure 8) (Sutherland, 1988). It is best developed in the southern part of the Arkoma Basin and displays marked increases in thickness on the down-thrown sides of the east-trending syndepositional normal faults associated with flexural downwarping of the south shelf margin (Sutherland, 1988) (Figure 10). The Middle Atokan sandstones are very fine to fine grained, lithic to sublithic arenites derived from erosion of the emerging eastern portion of the Ouachita and Appalachian orogenic belts (Sutherland, 1988). Middle Atokan sandstones have been interpreted as being deposited in "deep water" as a result of significant structural relief associated with the syndeposistional faults (e.g. Vedros and Visher, 1978; Sutherland, 1988). Houseknecht (1986) alternatively postulated that the sands were deposited below wave base but at comparatively shallow water depths (possibly on the order of 100 m) for the following reasons: 1) numerous widespread key beds display continuity across the associated syndepositional faults, and 2) there is no evidence of erosional truncation of strata upthrown by the faults. These lines of evidence imply that the rate of mud deposition kept pace with the rate

of subsidence and that the sea floor above the faults displayed little to no relief (Figure 11). Thus, deposition possibly occurred on a gently dipping, muddy slope lacking a bathymetrically distinct shelf-slope-rise geometry (Houseknecht, 1986). The Brazil and Red Oak are lenticular sandstones of limited areal distribution, and are elongated and oriented approximately east-west.

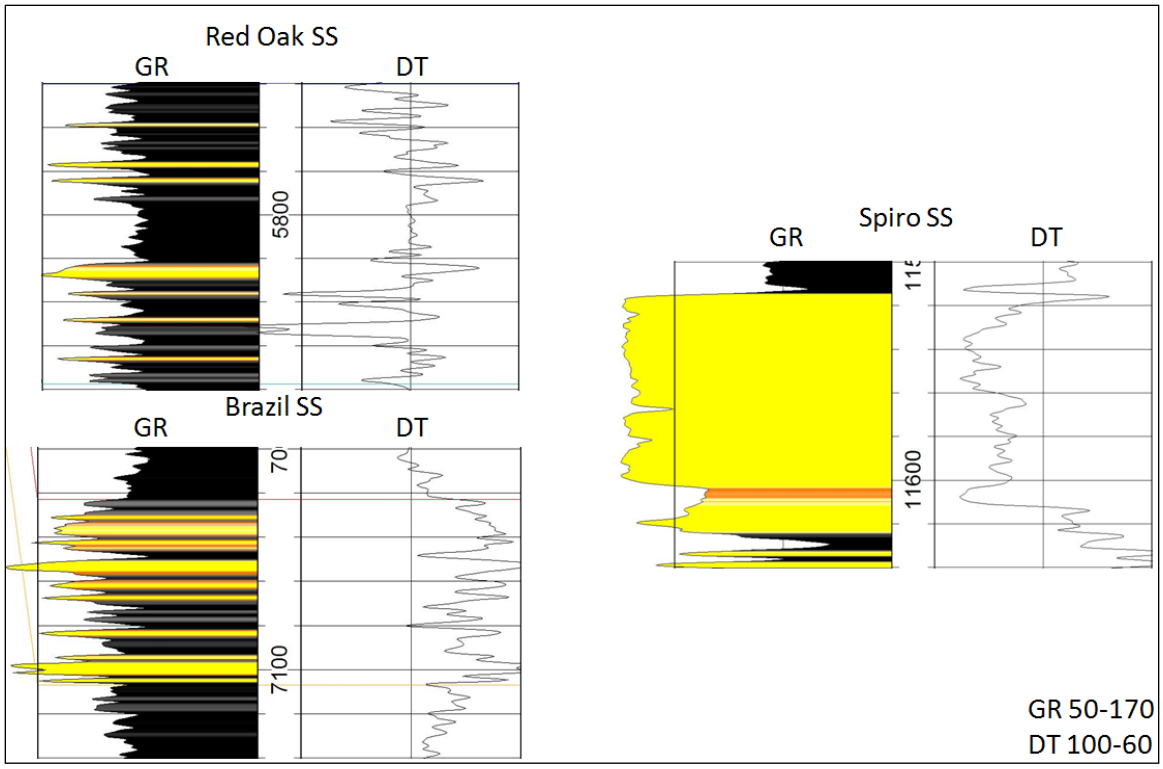

Figure 8. Log signatures of the Lower Atokan Spiro Sandstone, and the Middle Atokan Brazil and Red Oak Sandstones. GR=Gamma Ray (API) and DT=Sonic (µs/ft)

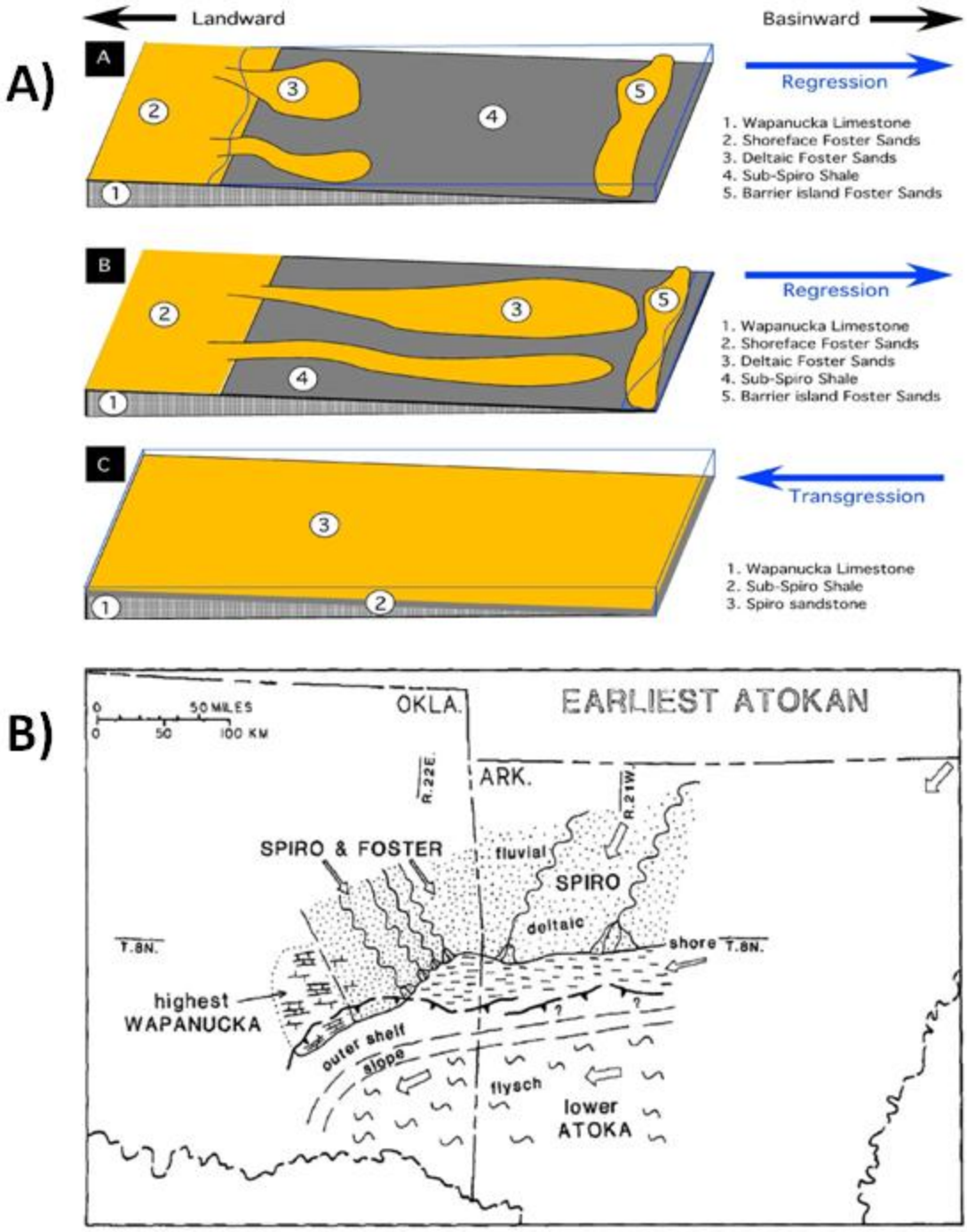

Figure 9. A) Depositional environment of the Spiro Sandstone (Sadeqi, 2007). B) Lower Atokan paleogeographic map (Sutherland, 1988).

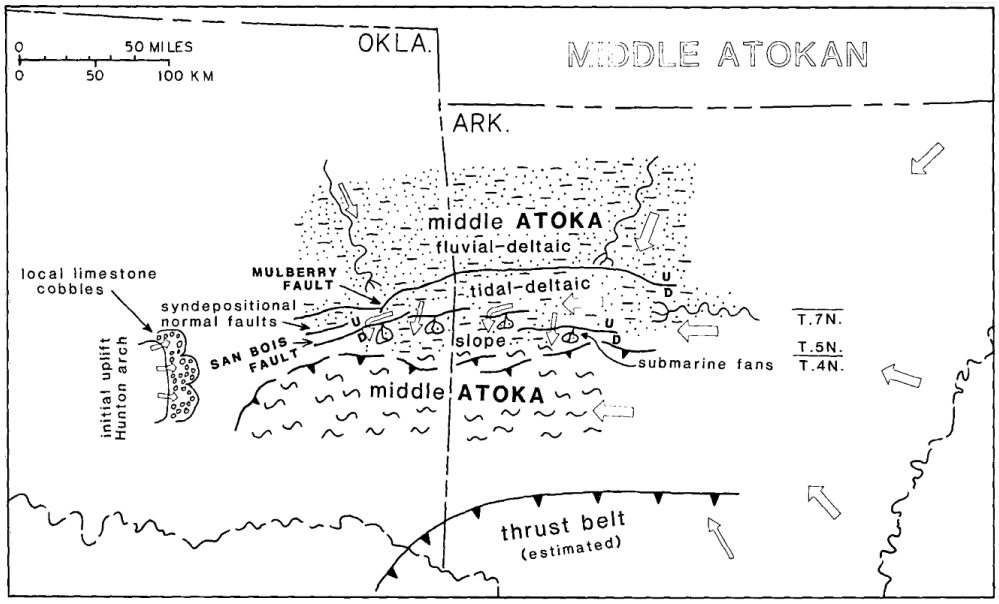

Figure 10. Middle Atokan paleogeographic map (Sutherland, 1988).

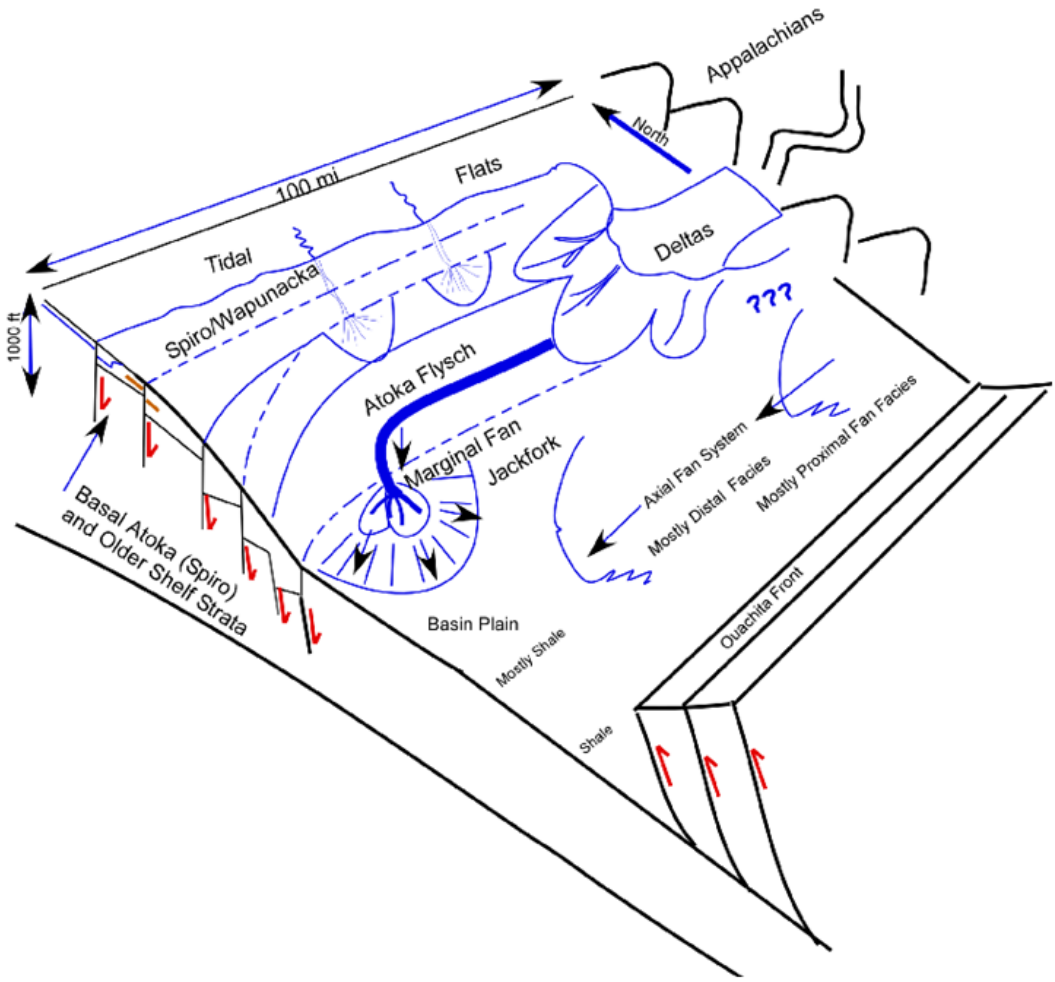

Figure 11. Paleogeologic reconstruction of the depositional environment of the Middle Atoka Formation (Çemen et al., in prep.).

CHAPTER 5

SEISMIC INVERSION

The 3-D seismic data used in this study have been inverted for acoustic impedance. Seismic inversion for acoustic impedance is linked to petrophysical properties. The use of inversion methods provides a quantitative means of extrapolating 1-D borehole measurements to a 3-D volume imaged by the seismic experiment by analyzing the relations between the well data and the seismic data (Leiceaga et al., 2011). Inversion for rock properties is a powerful tool for characterizing reservoirs and predicting lithology.

In seismic inversion, the goal is to remove the effect of the wavelet within the seismic data and recover physical rock properties (Leiceaga et al., 2011). Inversion data can therefore be used to interpret the top and base of a lithologic unit with better accuracy, and thus be used to map thickness changes in rock units as well as better understand changes in rock properties such as porosity.

Theory

A seismic trace is the convolution of three main components: the earth reflectivity; the seismic wavelet; and noise (Al-Moqbel, 2002). The resolution of the seismic trace is much lower than that of the real earth reflectivity. The band-limited seismic trace is produced by the convolution operation. This resolution is recovered by obtaining the reflectivity through a deconvolution operation (Robinson and Silva, 1978), in which the effect of the source signal in the seismic data is removed. In seismic inversion, this operation is constrained by establishing a relationship between the well data and the deconvolved seismic data. Deconvolution removes the effect of the wavelet by extracting it, leaving the reflection coefficient. The reflection coefficient is then ideally a series of spikes at each bed interface (Figure 12). The 2-D reflection seismic derived reflection coefficient (low frequency) is then calibrated to well control (high frequency). The resolution of the inversion data is improved allowing for the imaging of thinner beds and the derivation of some lithologic control away from well control (Hager, 2009).

The inversion data was modeled using a deterministic inversion based on simulated annealing (Garcia, 2012). Deterministic inversion uses well data and seismic to create a broad bandwidth impedance model of the Earth (Francis, 2006), and produces two sets of data: a relative and absolute impedance data set (Pendrel, 2001). The simulated annealing method is based on an analogy between the model-algorithm system and a statistical mechanical system (Garcia, 2012). The relative impedance data set has no low frequencies added, whereas the absolute data set has a low frequency model added (explained in detail below). The seismic data

used for interpretation in the study area were an absolute impedance data set with a low frequency model added (Garcia, 2012). A well containing velocity and density data is used to compute the low (below seismic band) frequency part of the inversion spectrum in order to increase the bandwidth of the data (Pendrel, 2001). This involves attempting to recover the acoustic impedance as a function of depth (or time) from observed normal incidence seismograms (Francis, 2006).

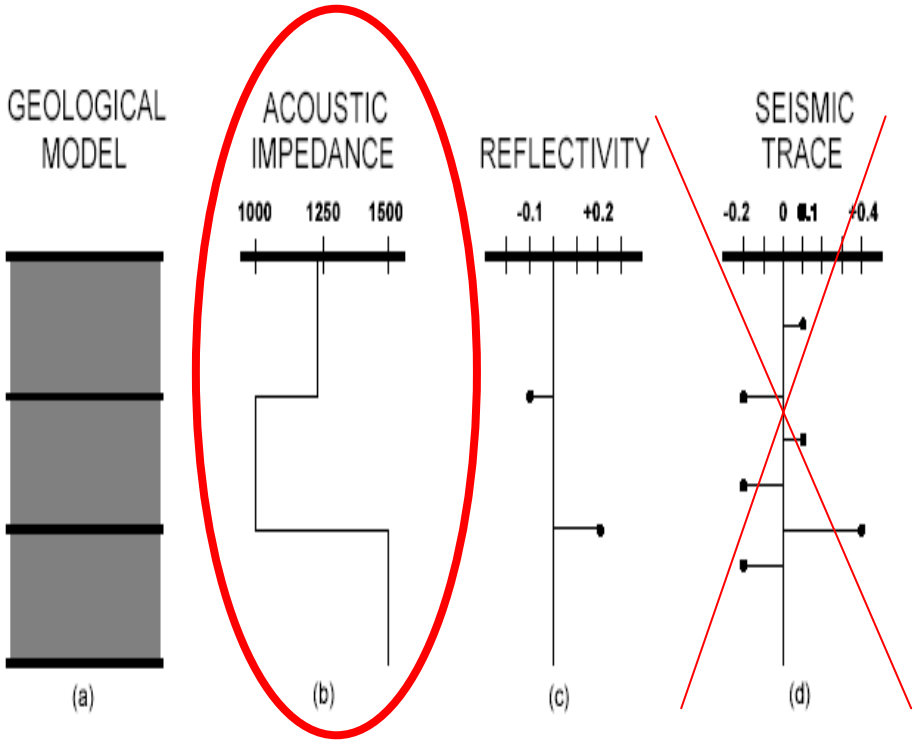

Figure 12. A non-specific example of an inversion model where (a) is a three layer Earth model, (b) acoustic impedance, (c) reflection coefficients (d) convolution of reflectivity series with a wavelet. Remove the effect of the wavelet to get back to acoustic impedance (Modified Hampson -Russell, 1999).

Process of Inversion

An inversion problem refers to a mathematical process used for determining the physical properties of a system characterized by a set of model parameters, given the observed response of the system. In seismic inversion for rock properties, the observed response of the system refers to the seismic and well data; the model parameters refer to the subsurface acoustic and elastic properties (Leiceaga et al., 2011). The mathematical objective of an inversion algorithm is to minimize the objective function, which is a measure of the difference between calculated and observed data. Convolution generates a seismic response by convolving the earth model with a wavelet. Seismic inversion simply uses an inverse algorithm to get back to the earth model (Banihasan, 2006).

As summarized by Castagna (2007), inversion comprises three basic components: a) converting seismic amplitudes to reflection coefficients; b) calculating acoustic impedance contrasts from the reflection coefficient; and c) converting the impedance changes to absolute impedance by the addition of a low frequency model. In detail, there are many additional steps involved in the inversion process (Figure 13). These include data quality control, log calibration (well conditioning), wavelet estimation, generation of a low frequency model, and finally the inversion.

The first step is to study the quality of the data (i.e. horizons, logs, and seismic). Quality control includes removing erroneous data from the sonic and density curves, and generation of missing curves (acoustic impedance). The second step involves log analysis and depth to time

conversion (Garcia, 2012). The third step is wavelet estimation, which is done by extracting a wavelet from the seismic data (Hager, 2009).

Wavelets are estimated for the seismic volume as the convolutional operator between the calibrated reflectivity logs and the seismic data (Schlumberger, 2009). There are three methods that are commonly used to calculate the wavelet that are imbedded in the data (Hampson-Russell, 1999). The first method is "purely deterministic," which would measure the wavelet directly using surface receivers. The second method is "purely statistical," which would derive the wavelet from seismic data alone. This method, at times, is unreliable because it is sometimes hard to determine the phase spectrum. The third method is using a well log, which would ideally tie perfectly or almost perfectly to the seismic data (Figure 14). The reflectivity is calculated at the well using the density and velocity log curves. The reflectivity is then converted from depth to time using checkshot surveys, bulk shifts, and visual ties, so that the synthetic well log data can be compared to the seismic data (Figure 14). The correlation between the well reflectivity and the seismic trace at the well location is used to solve for a wavelet, which gives a representation of the amplitude, frequency, and phase of the seismic data (Garcia, 2012). The third method may not produce a good wavelet extraction if the tie is not exact, resulting in a poor depth to time conversion.

Wavelets can change from trace to trace as a function of time, so the optimum wavelet extraction method is to find an "average" wavelet for the entire seismic data cube (Hampson-Russell, 1999). For this study, a constant phase wavelet was extracted using the well log method (Figure 14) (Garcia, 2012). A constant phase wavelet is extracted by calculating the amplitude spectrum from the seismic. This type of wavelet extraction tends to be most robust where there are imperfect well ties (Hampson-Russell, 1999). The parameters that have the most impact on

wavelet quality include conversion of the log calibration to the time domain (by generating well-to-seismic ties), the method of extraction (and subsequent amplitude and phase assumptions), the analysis window, and to some degree, the length of the wavelets (Leiceaga et al., 2011).

The fourth step is adding the low frequency model (LFM) to the data, which is the starting point of the inversion process (Garcia, 2012). The role played by the LFM is to fill in the lowest frequency gap (Figure 15) left by most conventional seismic data acquisition methods (~0 to 10 Hz) in order to increase bandwidth. A low-pass filter is applied to the well data (0-500 Hz), and low frequencies are interpolated and extrapolated at the well locations in order to populate the entire 3D seismic geometry (Leiceaga et al., 2011). The LFM (0-10 Hz) is added to the seismic bandwidth (8-80 Hz) in order to produce a full bandwidth inversion. The purpose of the LFM is to attain an absolute impedance model for the subsurface. Medium and high velocities yield a relative acoustic impedance model, and therefore are not a true acoustic impedance model for the subsurface (Garcia, 2012).

After these steps are taken, the seismic data is ready to be inverted for acoustic impedance. The inversion process is a deterministic approach, which converts seismic data from interface properties to layer properties. The inversion is based on a convolution model. This model generates synthetic seismic data via an iterative process, which seeks to reduce the error between observed and modeled seismic. The inversion estimates the physical properties, and the reflection coefficients are calculated and convolved with the appropriate wavelet in order to compare the modeled seismic with the measured seismic data (Leiceaga et al., 2011). When the inversion process is completed, calculated acoustic impedance curves, from well data, are compared to the seismic for quality control (Hager, 2009).

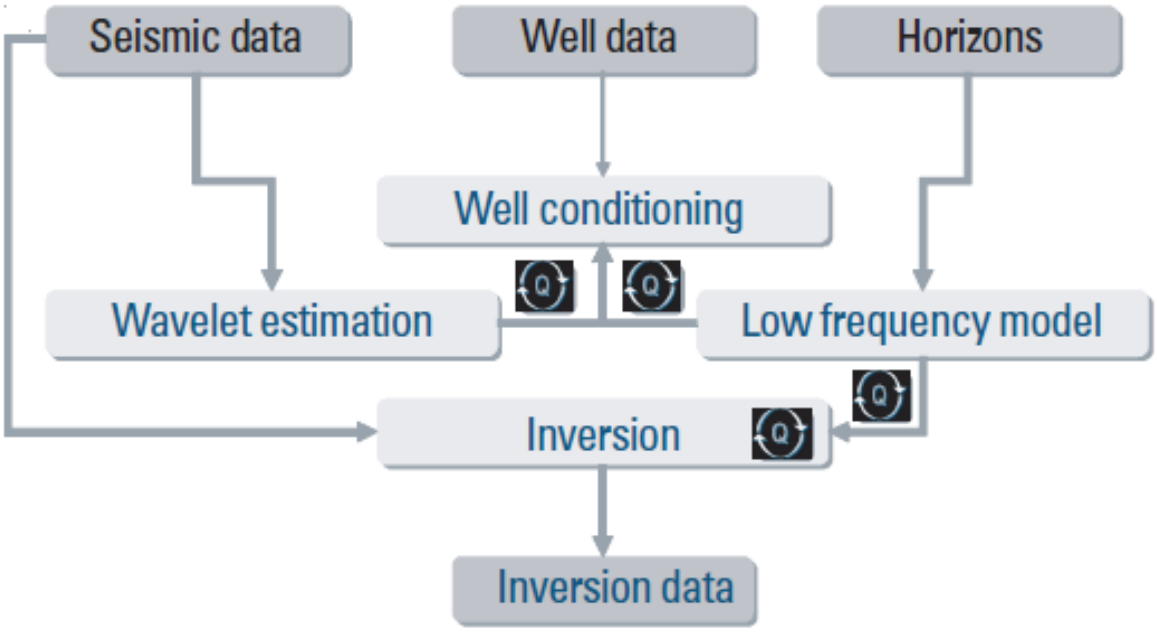

Figure 13. Fundamental workflow of seismic inversion (Leiceaga et al., 2011).

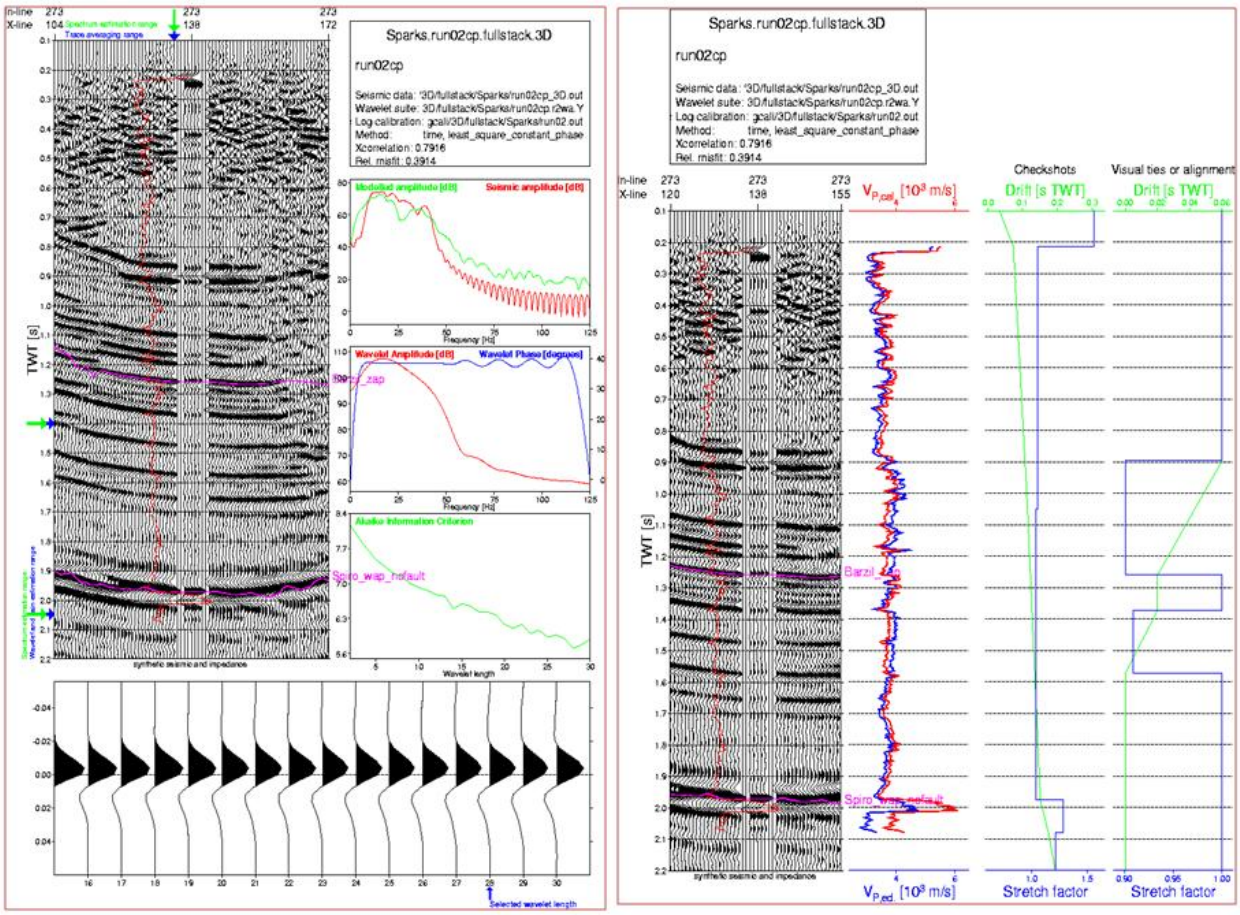

Figure 14. Well calibration to perform a fullstack constant phase wavelet extraction from the data using a check shot, 40.0 ms bulf shift, and visual ties (Garcia, 2012). Red line on seismic section represents synthetic ties. The sonic log is being edited where checkshots and visual ties exist, and is colored blue with the original shown in red.

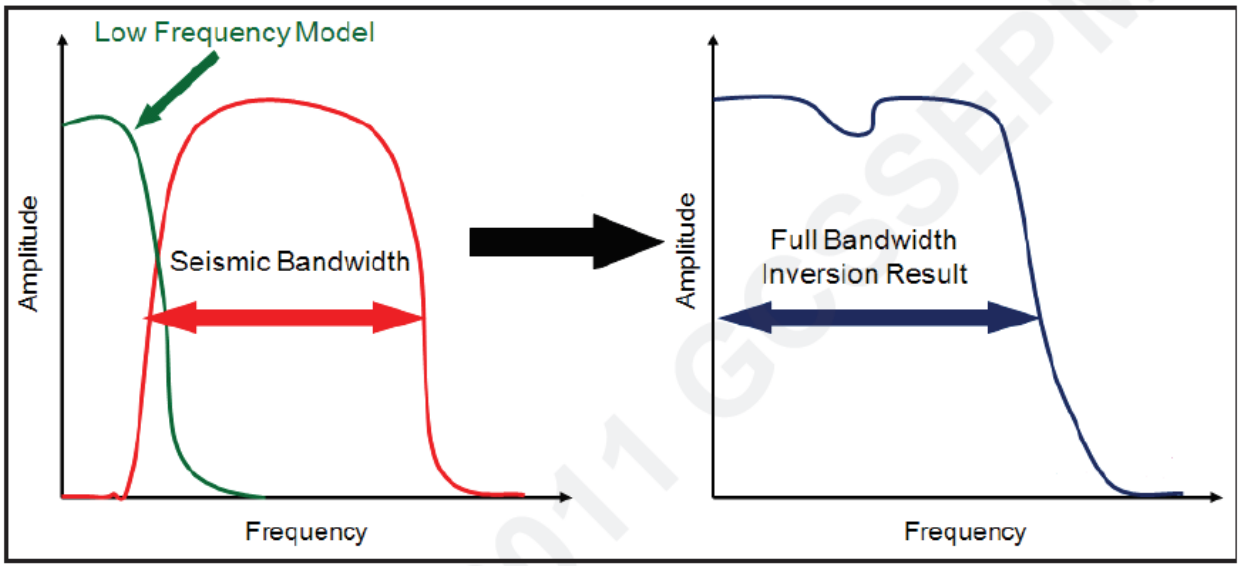

Figure 15. Generalized amplitude spectrum of seismic data and the low frequency model. The primary purpose of the low frequency model is to fill in the low frequencies that are generally missing in seismic data (~0-10 Hz). The low frequency model is calculated from the available well log data, interpreted horizons, seismic dip and interval velocities, and serves as the initial model in the inversion iteration process (Leiceaga et al., 2011).

Seismic Acoustic Impedance versus Well Log Acoustic Impedance

Three well logs, calibrated to seismic, were used for the inversion (Garcia, 2012) (Figure 16). These logs included sonic and density logs. One well also included a checkshot survey. A checkshot survey is generated with a receiver located in the borehole at a known depth. After a source has been generated at the surface the time to reach the receiver is recorded (Schlumberger, 2009). The depth and time are known values and can be used to calibrate a sonic log.

To check how calculated acoustic impedance from well logs compare to seismic acoustic impedance values, cross-plots of average seismic and well log acoustic impedance values in the Brazil and Red Oak Sandstones were generated (Figure 17). Average seismic and log values had to be used because of the vastly different sample rates and resolutions of seismic data and well log data. The sample interval of the seismic data is 4 ms, which is approximately every 18 feet assuming a velocity of 4,500 ft/s, and well logs values were sampled every 0.5 foot.

Due to the wide range of velocities used for inverting the seismic data, there is a lack of correlation between calculated acoustic impedance from well log values and seismic acoustic impedance (Figure 17). The low frequency model can affect the values of acoustic impedance away from wells that were used in the inversion process. An example of a well with a poor low frequency model is well 3 (Figure 18). Low frequencies travel much deeper than higher frequencies and thus are not recorded by surface seismic due to attenuation. Addition of the low frequency model is important for an accurate inversion. With only three wells and seismic data

used for the inversion, a great deal of interpolation was made between wells (Hager, 2009). If more wells contained density logs and sonic logs, this issue may be resolved. Some examples of where the well log calculated acoustic impedance and seismic acoustic impedance differ significantly are shown in Figure 19. In general, the seismic data has underestimated the acoustic impedance values compared to the calculated acoustic impedances generated from log data. However, lower acoustic impedance values seen in seismic do correlate to lower acoustic impedance values calculated from well logs.

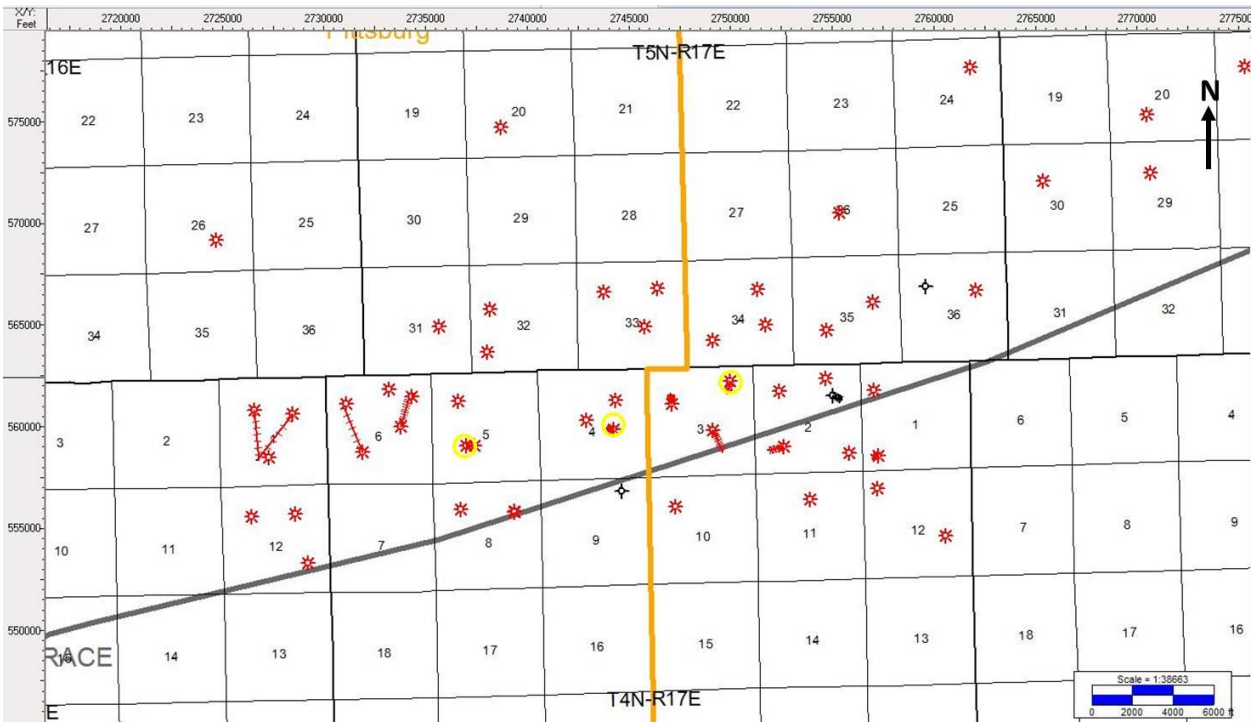

Figure 16. Map showing distribution of well control across the study area. Wells circled in yellow were used for the seismic inversion.

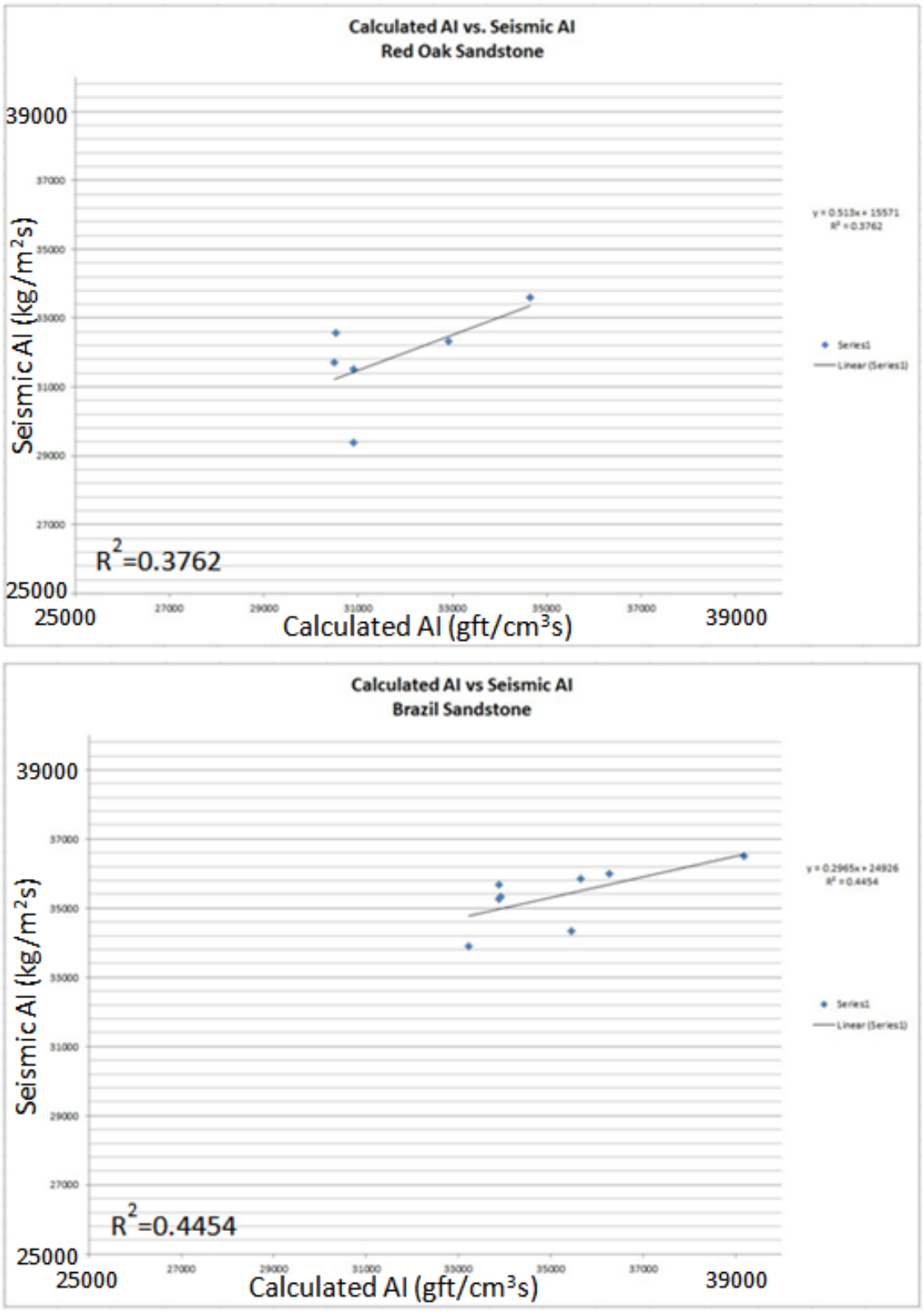

Figure 17. Charts showing acoustic impedance from seismic versus calculated acoustic impedance from well log data.

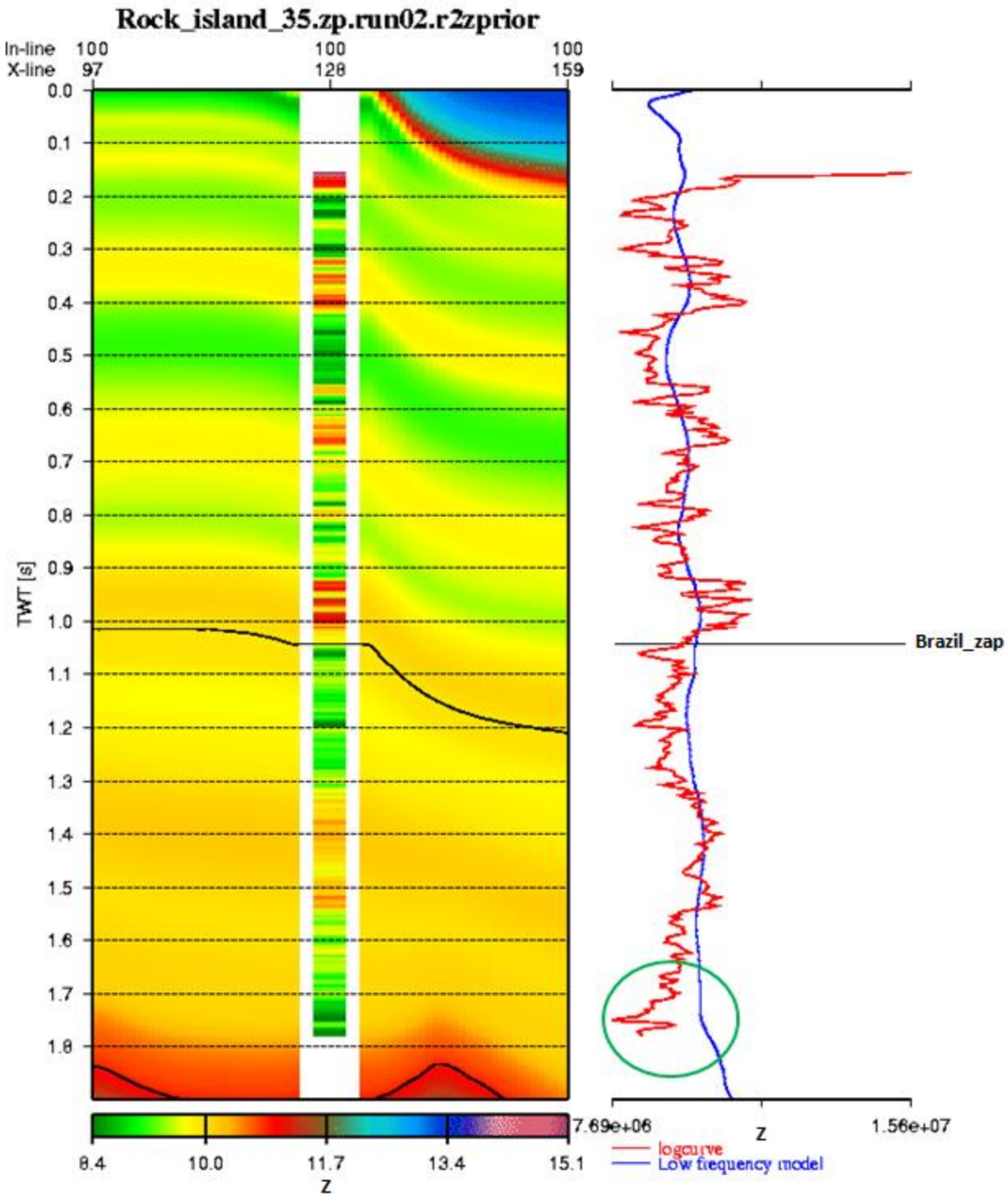

Figure 18. Green circle indicates where the low frequency model (blue line) and calculated acoustic impedance curve values (red line) do not match. Color scale for seismic inversion is in kg/m^2s. Log curve scale in gft/cm^3s (Garcia, Odegaard America Inc, 2005).

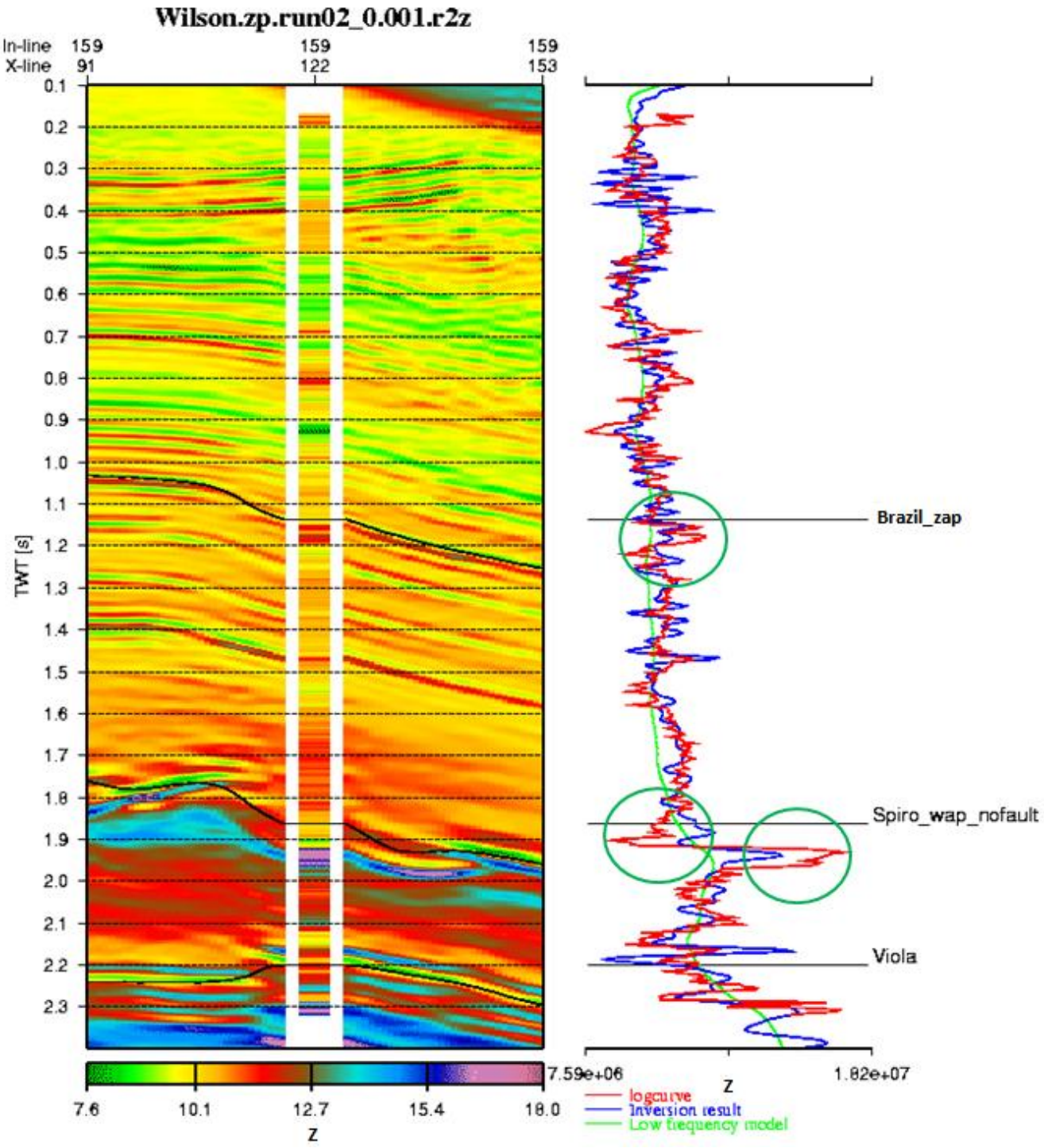

Figure 19. Green circles indicate areas where the seismic acoustic impedance result (blue line) and log curve acoustic impedance (red curve) do not match. Color scale for seismic inversion is in kg/m m^2s. Log curve scale in gft/cm^3s (Garcia, Odegaard America Inc., 2005).

Applications

Acoustic impedance inversion data is commonly used in industry to predict facies changes correlating to higher porosities (Figure 20). Calderon and Castagna (2007) concluded that changes in seismic amplitude response at the reservoir in Balcon Field in Columbia could be related to lithologic and porosity changes in areas of good seismic quality (Figure 20A). The velocity-porosity and impedance-porosity relation for the Caballos Formation in Balcon Field was improved when data were sorted by clay content and lithologies were included as a constraint. Calderon and Castagna (2007) determined that acoustic impedance is the most significant attribute to predict porosity and lithology in the Caballos Formation, and changes in impedance derived from seismic inversion are related to changes in porosity and/or lithology in Balcon Field.

Pedersen-Tatalovic (2008) presented a method called "Event Based Low Frequency Impedance Modeling" to derive absolute impedance accurate enough to be used for porosity prediction in chalk in the Danish North Sea. The application of the method significantly enhanced the estimations of the absolute porosity (Figure 20B). Event Based Low Frequency Impedance Modeling is an automated procedure used to predict low frequency impedance data, making use of a range of seismic attributes. The tool allowed them to browse through a large number of attributes to find those that have an impact on accurate porosity prediction.

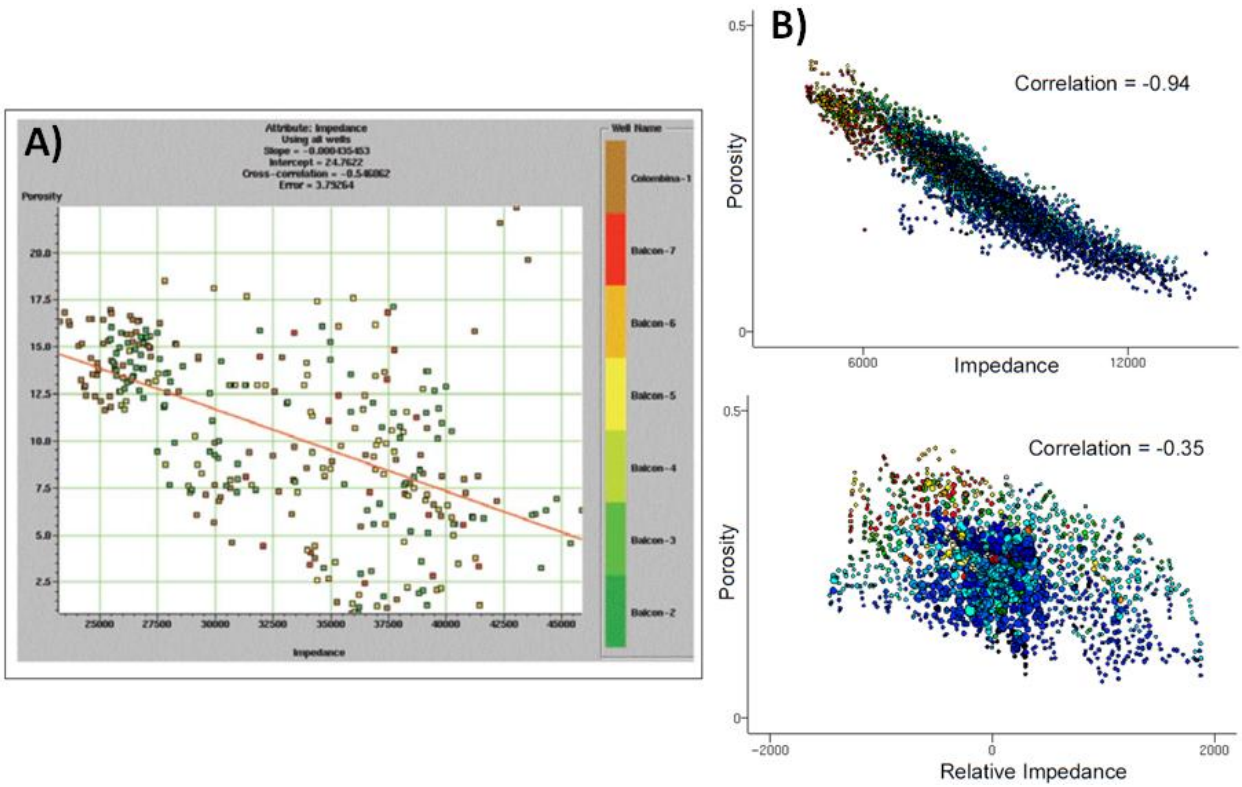

Figure 20. A) a cross-plot of porosity versus acoustic impedance with the color scale corresponding to different wells for Cretaceous aged sandstones in Magdalena Valley, Columbia (Calderon and Castagna, 2007). B) examples from the Danish North Sea (Pedersen-Tatalovic, 2008).Lower acoustic impedance values correlate to higher porosity values.

CHAPTER 6

INTERPRETATION OF THE SEISMIC INVERSION DATA

Previous Work

Parker (2007) and Sadeqi (2007) analyzed the Spiro Sandstone and Wapanucka Limestone as one seismic package because they were masked by one large peak on the conventional seismic reflection data (Figure 21). Hager (2009), using the inversion data, resolved the two lithologies (Figure 22) because: 1) the effect of the wavelet was removed, and 2) the large impedance contrast present between the slower, more porous Spiro Sandstone and the faster, less porous Wapanucka Limestone. Gamma ray logs, sonic logs, and calculated acoustic impedance curves, were tied to the seismic in order to distinguish the two lithologic units. By picking the Spiro as a unique unit, Hager (2009) was able to analyze the unit exclusively and determine how the thickness, structural position, and rock properties such as porosity, affected the acoustic impedance of the unit. Hager (2009) then correlated acoustic impedance to porosity where porosity logs existed, and determined that higher porosity caused a decrease in acoustic impedance because changes in acoustic impedance are directly related to the density and velocity of the rocks (Figure 23). In locations where the Spiro was more porous, the velocities were slower than where the Spiro was tightly cemented.

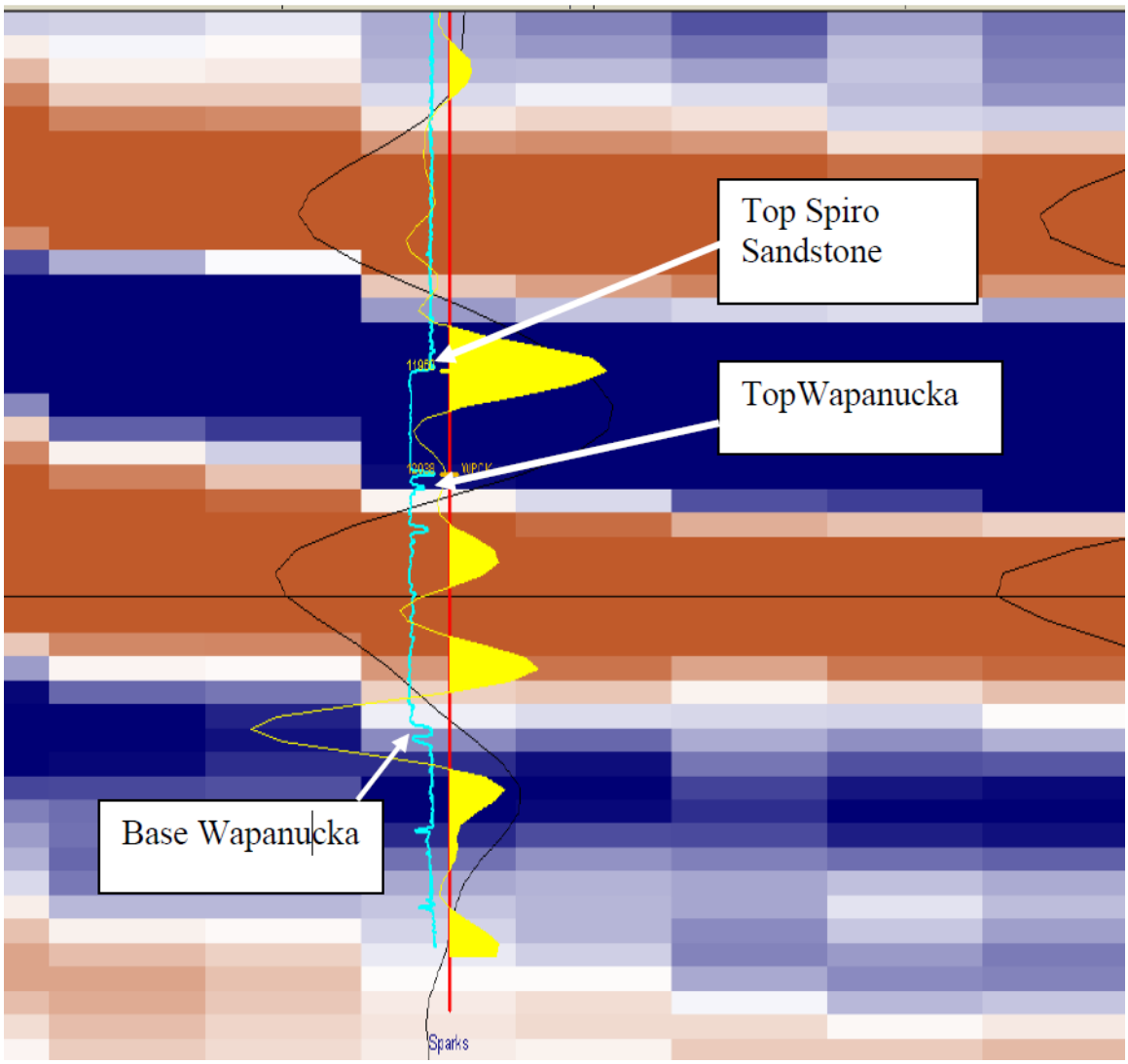

Figure 21. Pre-stack time migrated (PSTM) data resolving the Spiro Sandstone and Wapanucka Limestone as a single reflector. Blue represents peaks and brown represents troughs. The yellow curve is the synthetic (from high frequency well data) and the light blue is the gamma ray. The black curves in the background are the seismic traces overlain on the color filled seismic data (low frequency). The tops and bases of units are marked on the gamma ray curve. On the synthetic, the top of the Spiro is seen as a large peak and the base of the Wapanucka is seen as a large trough (Hager, 2009).

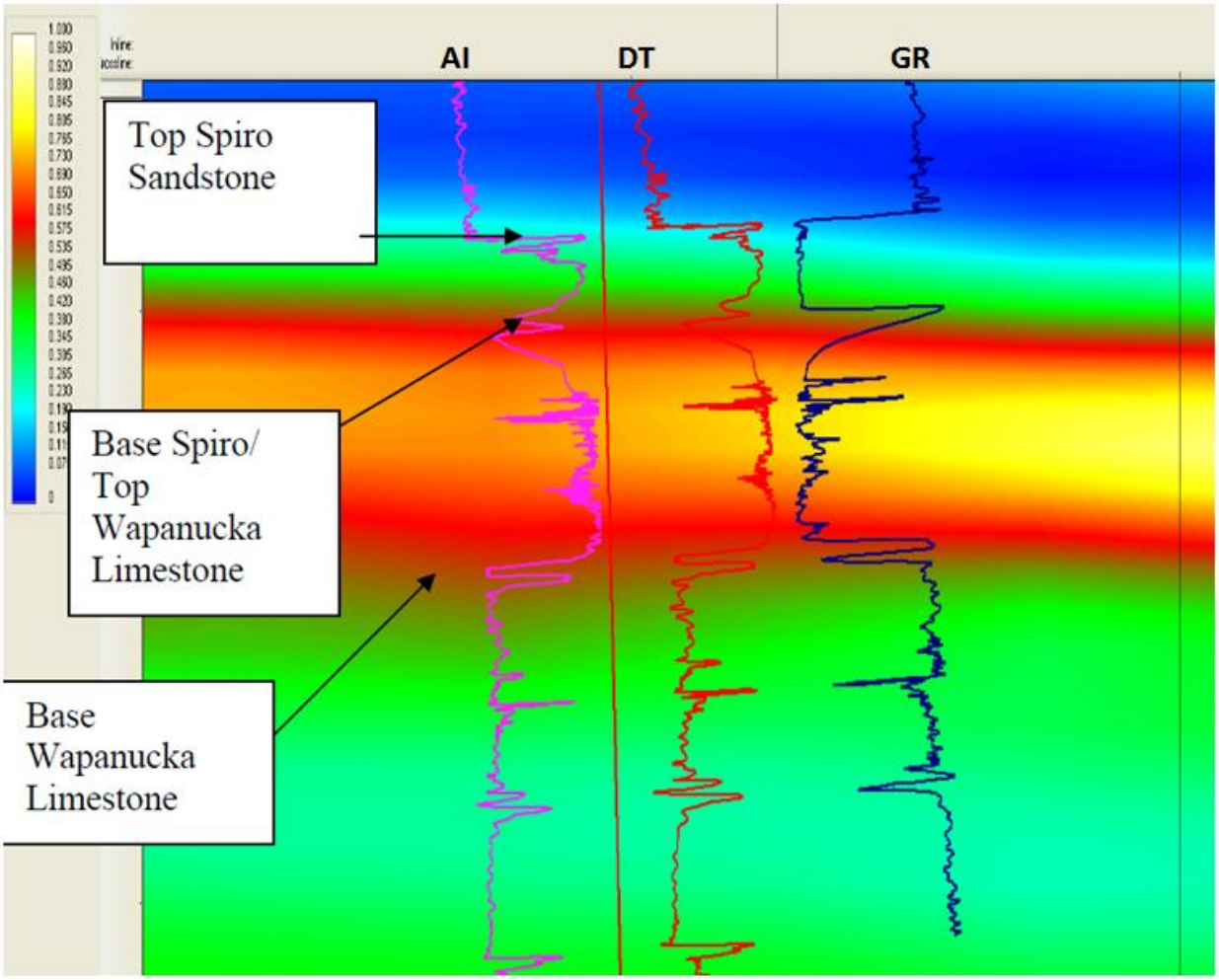

Figure 22. Inversion data allowed for the differentiation between the Spiro Sandstone and Wapanucka Limestone shown in a vertical display in KINGDOM Suite. The pink curve is the acoustic impedance calculated curve, the red curve is the sonic curve, and the dark blue curve is the gamma ray. The display is shown in two way travel time (TWT). The color bar is in acoustic impedance, 1= largest acoustic impedance value 0= lowest acoustic impedance (kg/m^2s) (Hager, 2009).

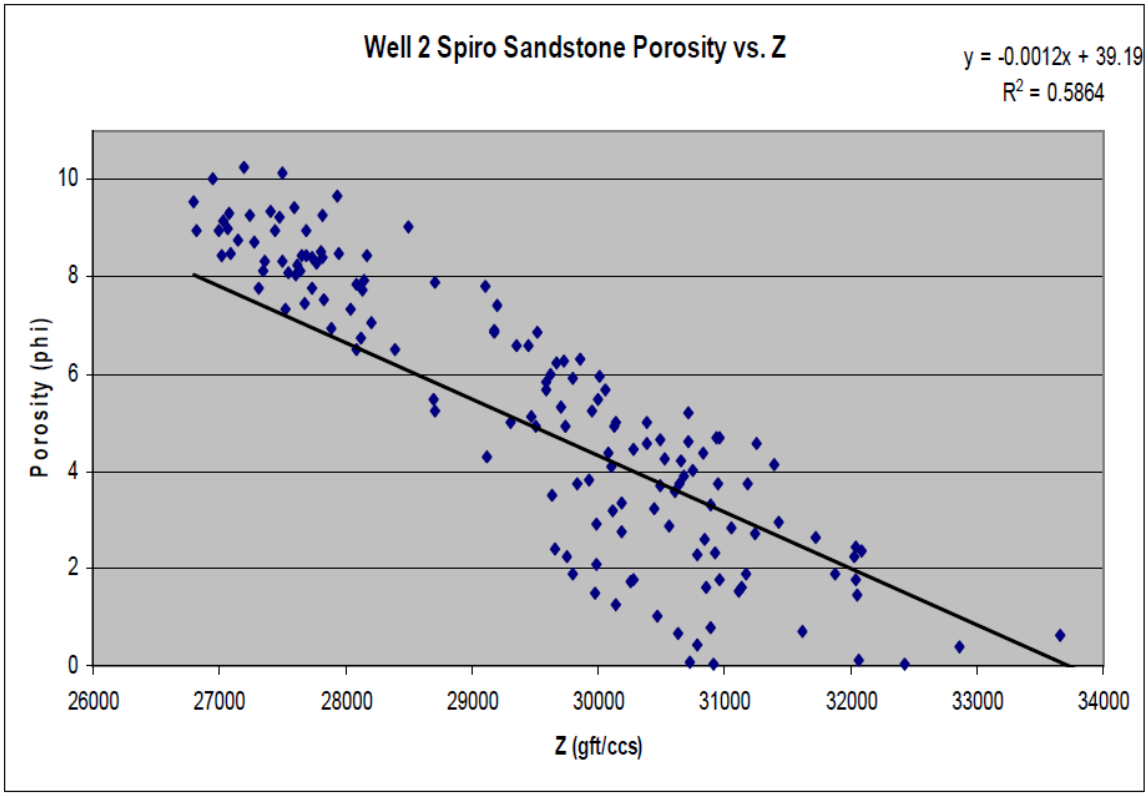

Figure 23. Cross-plot of porosity versus acoustic impedance for well 2. Correlation coefficient is 0.5864 (Hager, 2009).

Porosity

In the Brazil and Red Oak Sandstones, porosity ranges from 1 to 10%, depending on diagenetic features or fractures. However, the reservoir quality (i.e. porosity) is mostly a function of which slope channel deposits had sufficient clay grain coats emplaced to inhibit quartz cementation (Houseknecht, 1990). In areas where these diagenetic features are the reason for increased porosity, the acoustic impedance data can be used to predict porosity.

Rock properties, such as porosity, have a large impact on acoustic impedance (Hager, 2009). An acoustic impedance versus porosity cross-plot was generated from well logs for each interval (Figure 24). These plots show a linear correlation between porosity and acoustic impedance in the sandy portions of the Brazil and Red Oak Sandstones, and a fair correlation in the sandstone portions of the Brazil (R^2=0.781) and Red Oak (R^2=0.793) Sandstones. The shale sections displayed a poor correlation, Brazil (R^2=0.273) and Red Oak (R^2=0.212) Sandstones, most likely due to variation in properties such as mineralogy (Figure 25).

Maps of acoustic impedance values in the Brazil and Red Oak Sandstones were created using a volume attribute function (Figure 26). Data are extracted between two designated horizons (i.e. the top and base of the sands) and a root mean square value for acoustic impedance in the interval is calculated (Figure 27). Large areas of higher acoustic impedance are displayed in the center of the two maps (Figure 26), and well logs confirm this due to the formations containing more sand in these areas. The areas that contain more shale have slower velocities, yielding lower acoustic impedance values.

The cross-plots of the Brazil and Red Oak Sandstones suggest that there is a linear relationship between acoustic impedance and porosity in the sandy portions of the two rock units (Figure 24). However, using seismic inversion data as a predictive tool for porosity in areas with little or no well control would be very limited when applied to the Brazil and Red Oak Sandstones because of the large variation in shale content of the two units in the Arkoma Basin.

Due to the interbedded shale within these units, and the vertical resolution of the data, what appears as an area of higher porosity reservoir rock (sand) instead may be an area with a higher shale content. An increase in shale would increase the total porosity of the interval, thereby lowering the density and velocity, and ultimately lowering the acoustic impedance value for the interval. However, because shale has low permeability, it is not a good conventional reservoir, although it can be an excellent unconventional reservoir. The predictive capabilities of the seismic inversion data should be constrained to the parts of the two units that contain mostly sandstone. This is the reason that a good correlation existed between porosity and acoustic impedance in the homogeneous and blocky Spiro Sandstone (Hager, 2009).

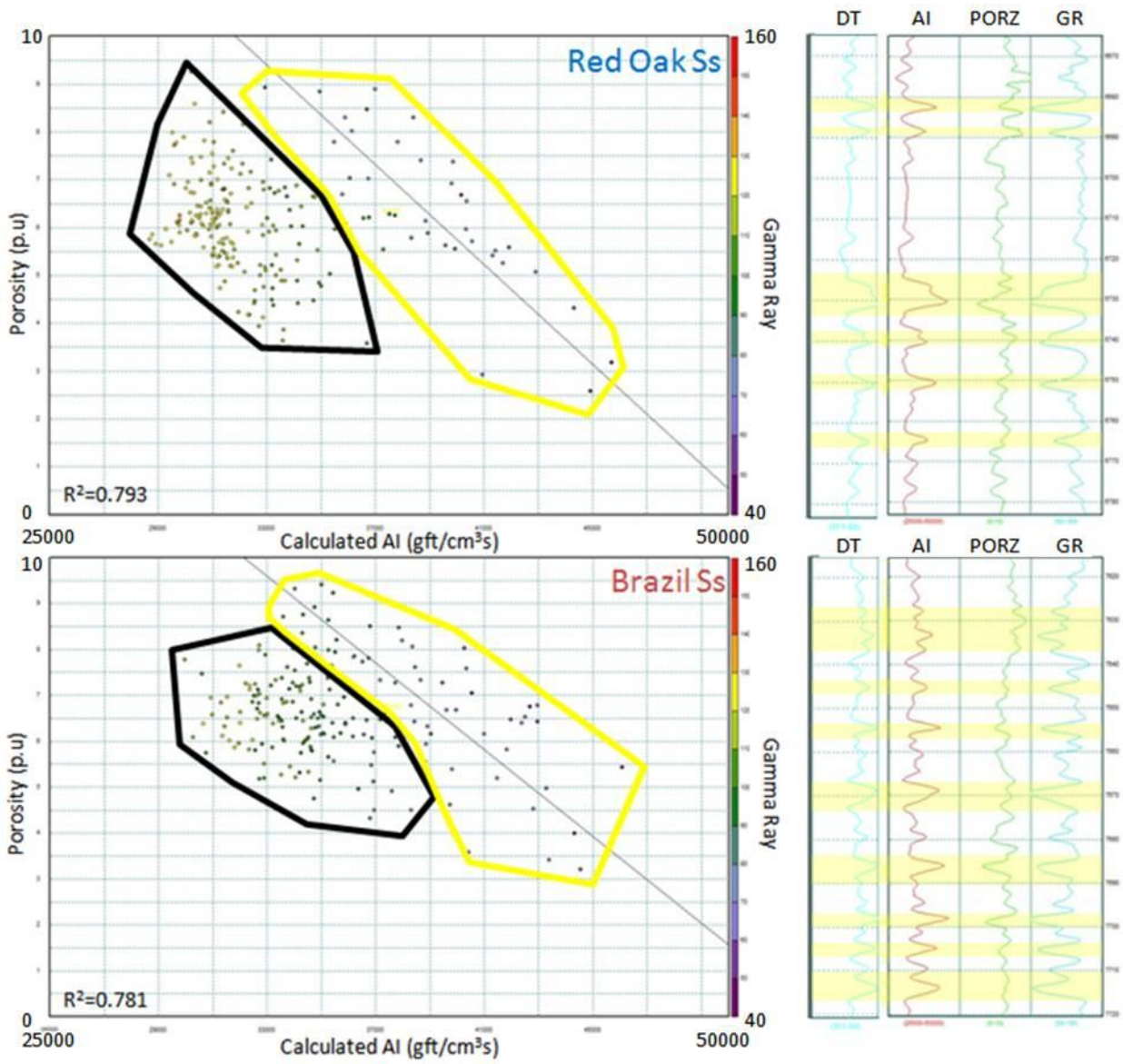

Figure 24. Cross-plots of porosity versus acoustic impedance for sandy portions of both intervals. Sand portions are marked with yellow on the logs. Points in yellow polygon are the sandy portions of the interval and points in black polygon are the shaly portions of the interval. SS=Sandtone DT=Sonic AI=Acoustic Impedance PORZ=Porosity GR=Gamma Ray

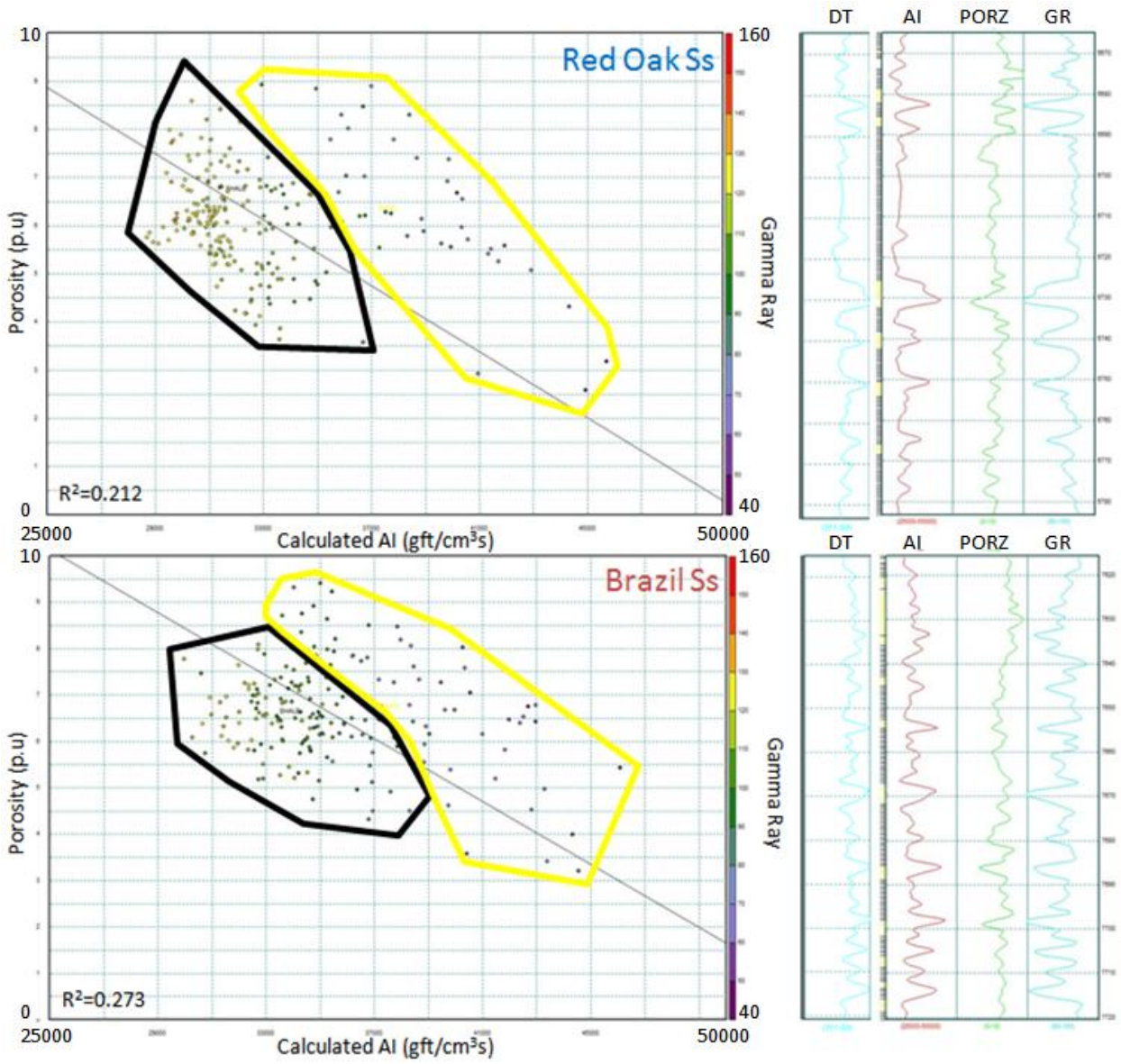

Figure 25. Cross-plots of porosity versus acoustic impedance for shaly portions of both intervals. Sand portions are marked with yellow ticks, and shale portions are marked with black ticks next to the well log. Points in yellow polygon are the sandy portions of the interval and points in black polygon are the shaly portions of the interval. SS=Sandtone DT=Sonic AI=Acoustic Impedance PORZ=Porosity GR=Gamma Ray

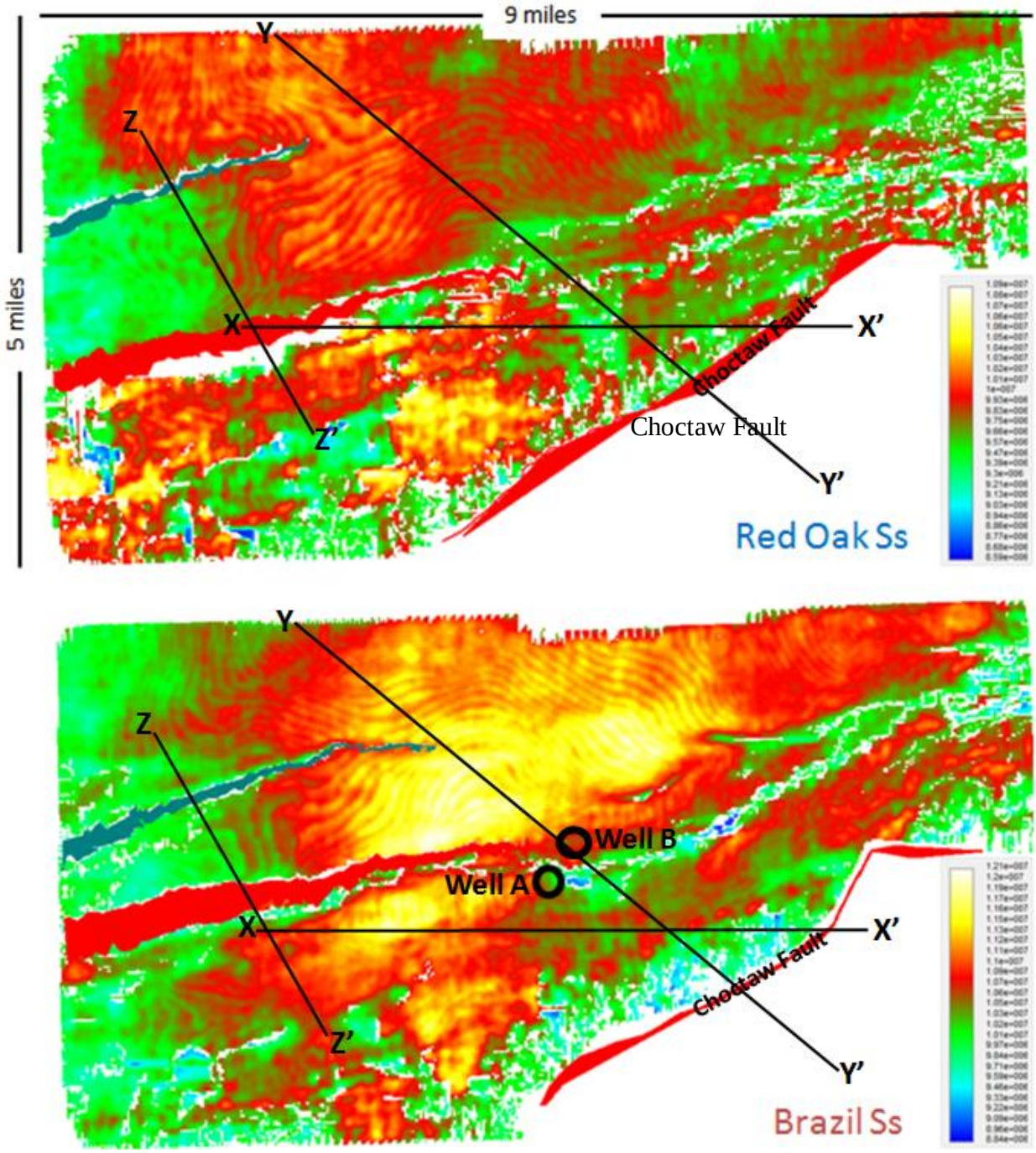

Figure 26. Acoustic impedance maps of the Brazil and Red Oak Sandstones. Cooler colors (blues and greens) indicate lower acoustic impedance values and warmer colors (reds and yellows) indicate higher acoustic impedance values. Color bar is in acoustic impedance units (kg/m^2s). SS=Sandstone. Notice the lower acoustic impedance region around the faults on the west side of the maps.

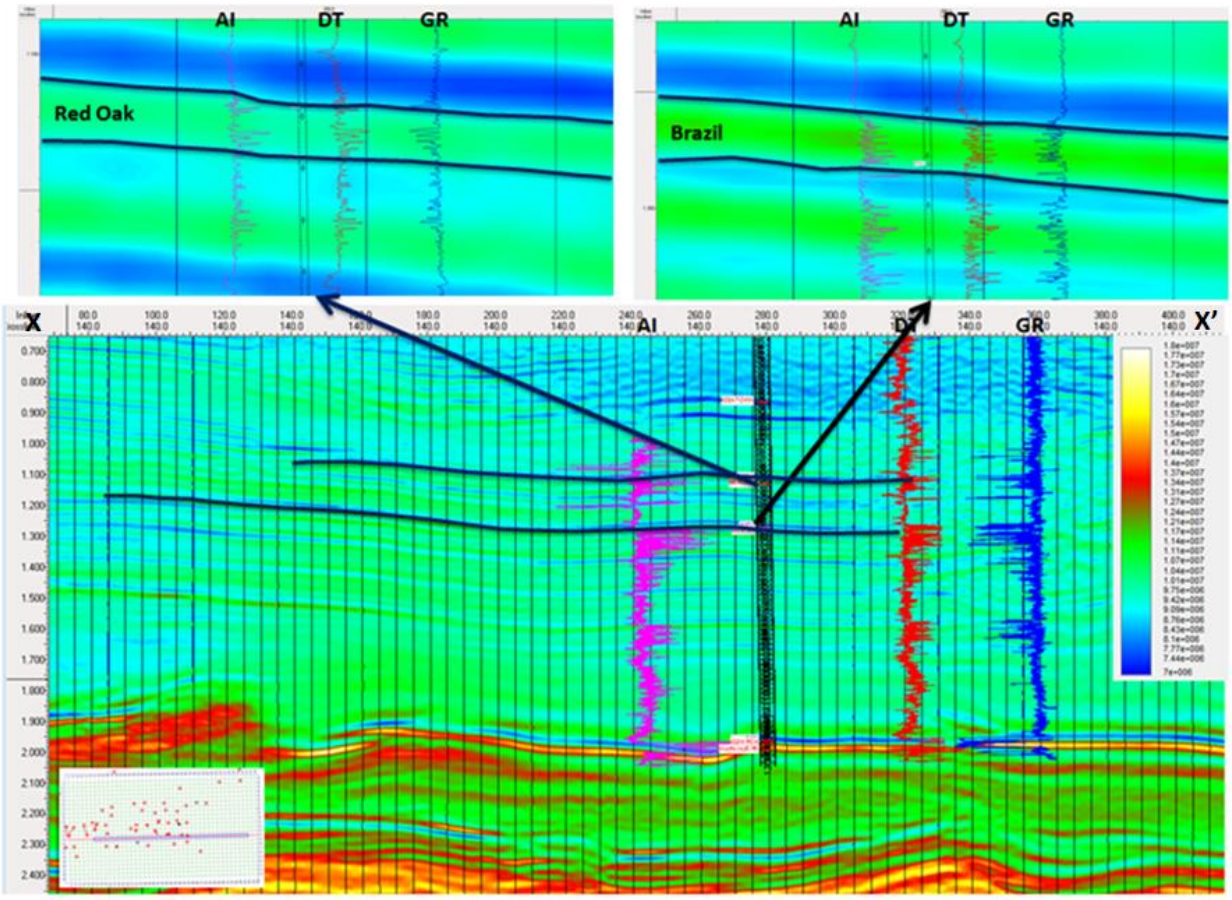

Figure 27. Line X-X' on figure 26. Horizons picked in acoustic impedance data. AI=Acoustic Impedance, DT=Sonic and GR=Gamma Ray. Lower acoustic impedance values (kg/m^2s) in blue and higher acoustic impedance values in yellow.

Structure

The Middle Atoka Formation is mildly deformed with broad folds and a few thrusts with little separation. Structure may not play a large role in controlling the productivity and associated porosity in the Brazil and Red Oak Sandstones. Impedance changes directly relate to rock property changes that are controlled by either structural or lithologic changes. Structural changes of the Atoka Formation were previously studied over seven seismic cross sections (Parker, 2007; Sadeqi, 2007). Cross section lines parallel (Figure 28A) and perpendicular to dip were analyzed. The dip lines showed rock property changes related to structural control. Arbitrary lines were drawn across the inversion survey approximately parallel to dip to illustrate relationships between structure and acoustic impedance (Figure 28B). Although the Middle Atoka is relatively undeformed compared to the lower unit, there are two major faults that cut the middle unit that may contribute to changes in acoustic impedance (Figure 29).

Using whole core from the Red Oak field to the north, Houseknecht (1990) concluded that permeability was enhanced in the Red Oak Sandstone by fracturing adjacent to thrust faults. In areas where the Brazil and Red Oak Sandstones have been faulted, it is possible that increasing porosity may be associated with a larger fracture density. Areas in between and adjacent to faults have lower acoustic impedance values, indicating that the faulted areas may have more porosity (Figure 26).

The goal of analyzing the structure was to infer if faulted regions may contribute to higher porosities. However, lower impedance values are not necessarily associated with fracture

porosity. Natural gas lowers the acoustic impedance of rock by replacing the water in the formation. For example, well A is near a fault in the Brazil Sandstone (Figure 26), and has low acoustic impedance, which could be caused by hydrocarbons in place based on its resistivity log compared to nearby (~1500 ft) well B (Figure 30).

All wells with sonic logs were analyzed to determine an average velocity for the Brazil and Red Oak Sandstones and where outliers existed in the survey (Figure 31). Velocity and acoustic impedance were cross-plotted to show that slower velocities would correspond to lower acoustic impedance values (Figure 32). In areas where wells contain faults, slower velocities are expected as well as lower acoustic impedance (Figure 26). Overall, acoustic impedance values did not consistently correlate with faulted areas. Using inversion data as a tool for determining fracture content is too ambiguous to use with any certainty in areas close to faults. This would assume that faulting caused fracturing which in turn increased porosity.

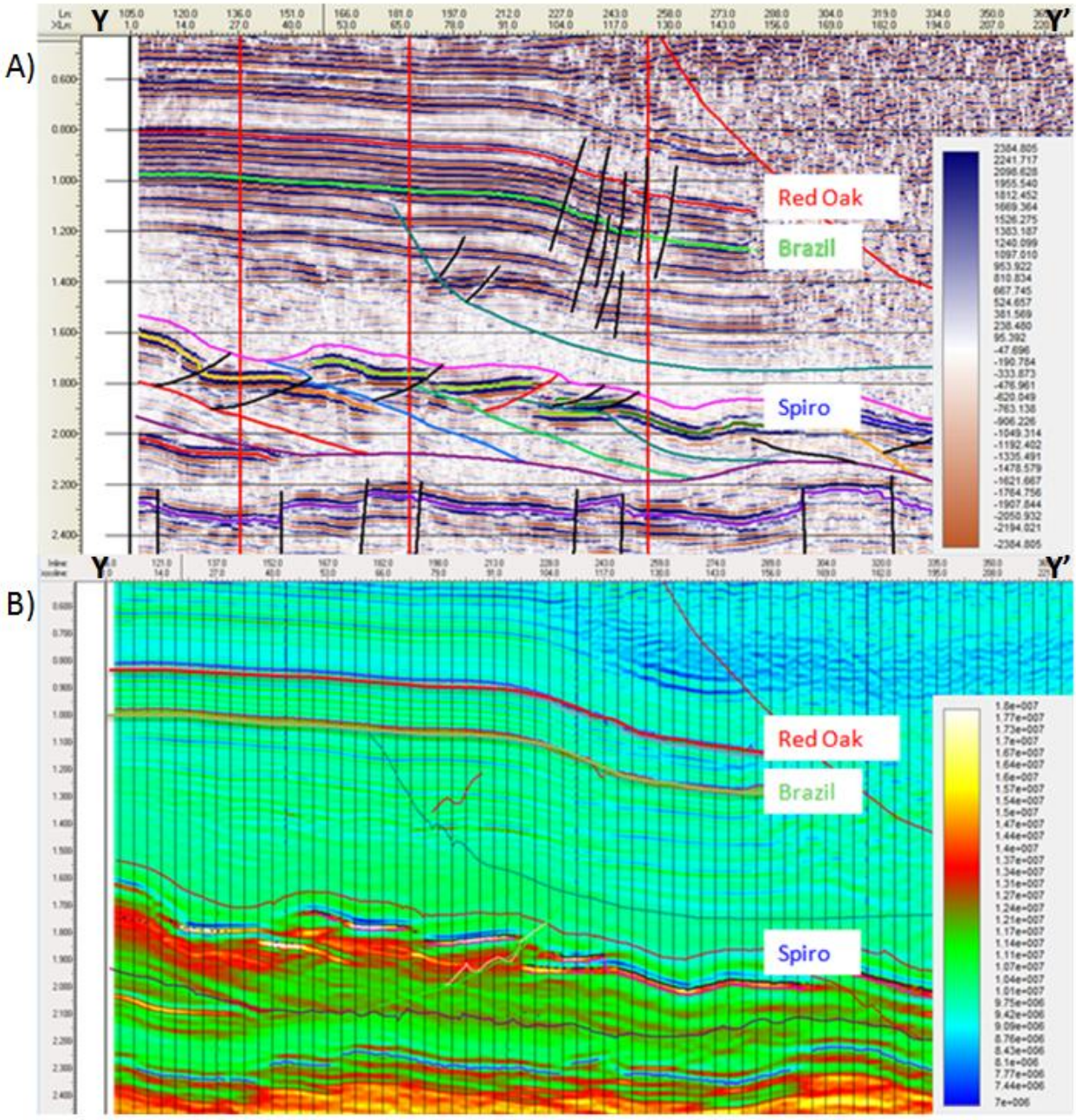

Figure 28. A) NW-SE dip line through the Wilburton gas field displaying a large thrust with an associated back thrust (Parker, 2007). B) Same line through inversion data. Y-Y' line from figure 26.

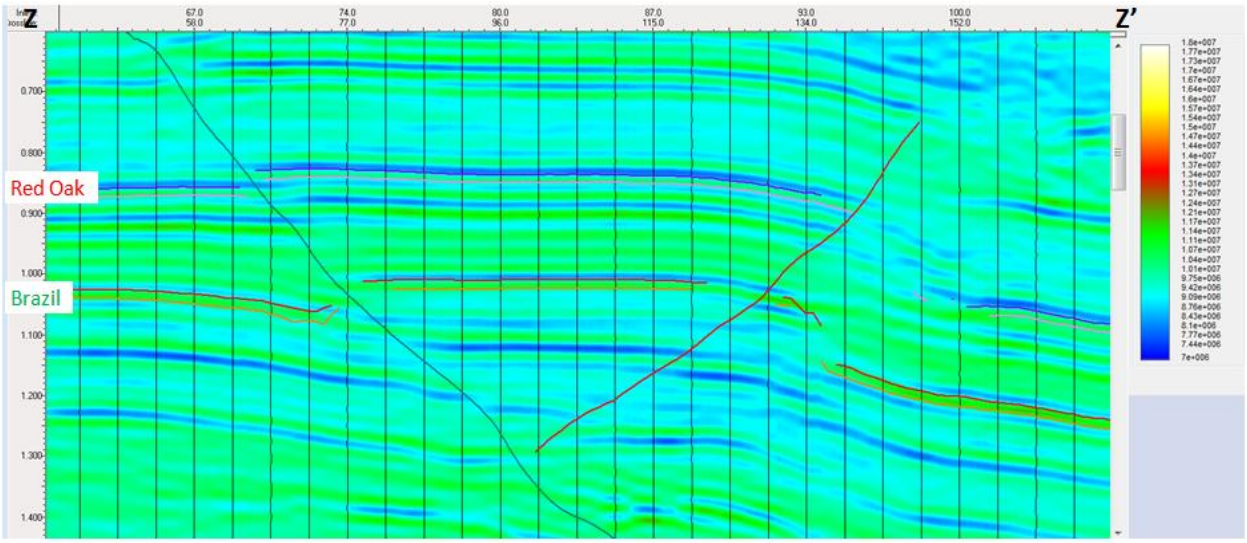

Figure 29. Cross section line Z-Z' from figure 26 illustrating the two major faults that cut the units in the survey area.

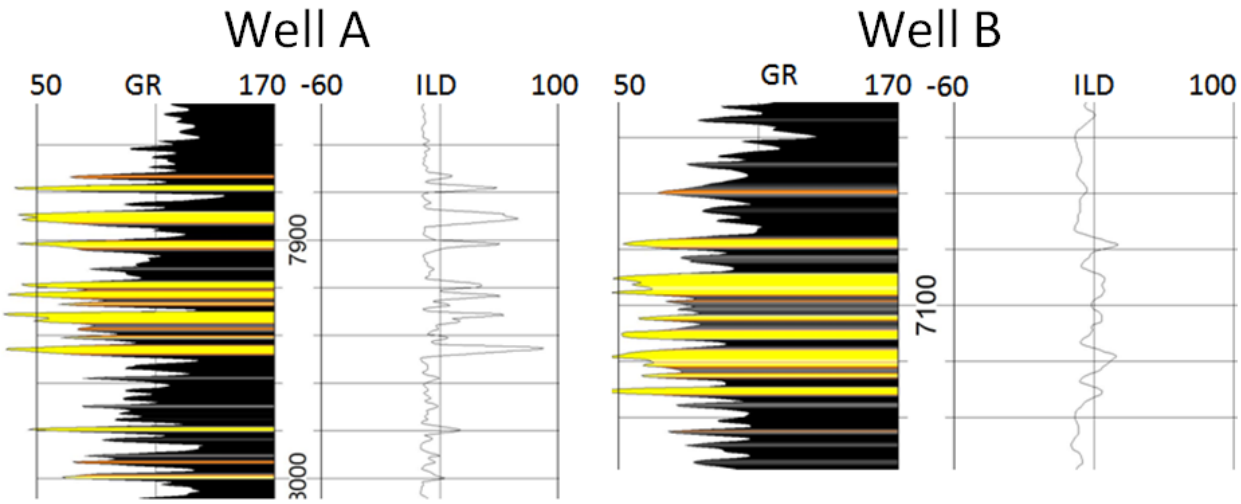

Figure 30. Brazil Sandstone resistivity log for well A versus neighboring well B on figure 26. GR=Gamma Ray and ILD=Resistivity.

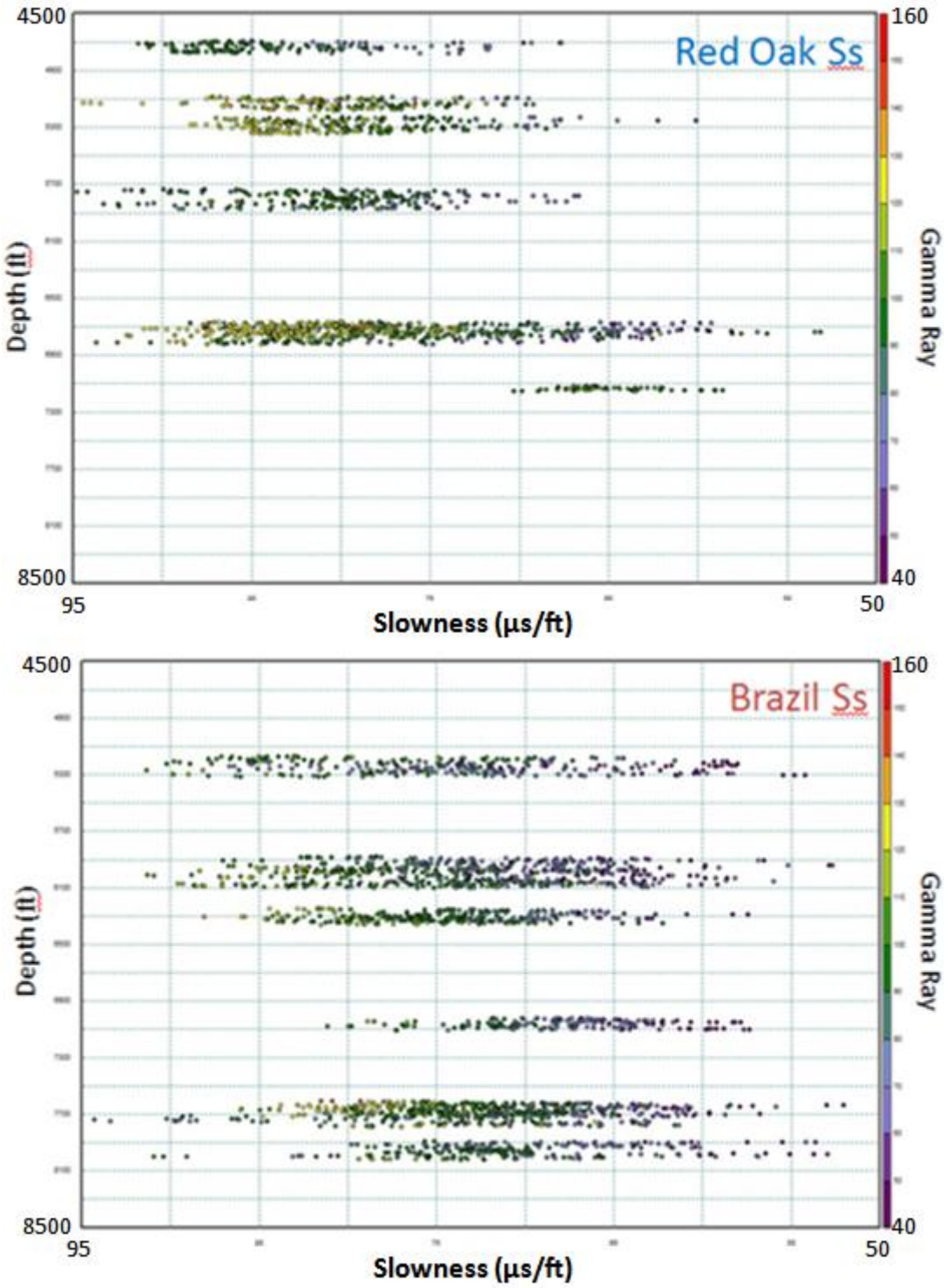

Figure 31. Sonic in the Brazil and Red Oak Sandstones versus depth for all wells with sonic logs. The units show a wide range of values with depth. SS=Sandtone

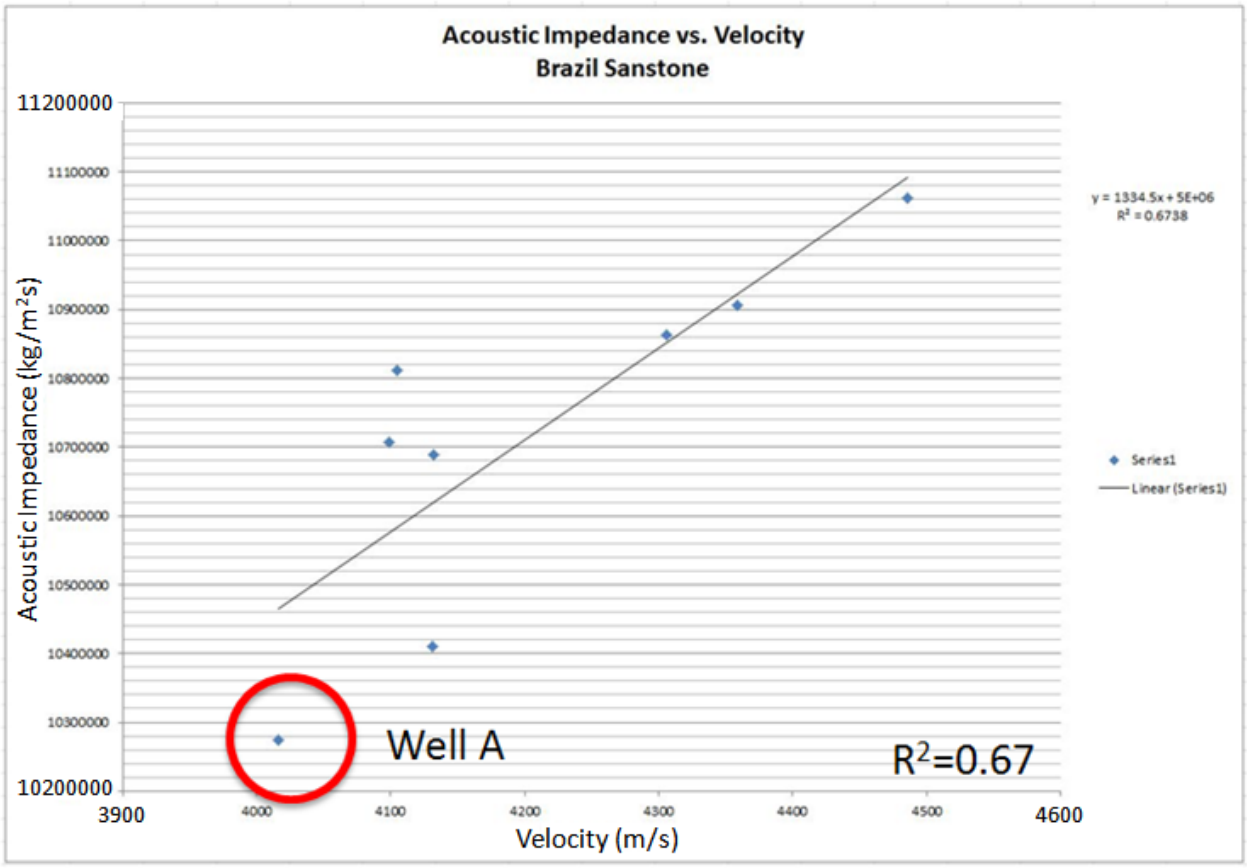

Figure 32. Average acoustic impedance values for the Brazil Sandstone interval cross-plotted against velocity for all wells that had sonic logs available. Notice well A has a slower velocity and acoustic impedance compared to the other wells.

Thickness

Thickness maps are important in determining the lateral and vertical extent of a reservoir. Generally, isochore maps are made from well log data and can be inaccurate in areas containing little well control. Seismic inversion data can enhance thickness maps by filling in the data between wells and thus yielding a more accurate interpretation. Because the masking effect of the wavelet is removed in the inversion process, the resulting data are much nearer to the actual geologic model. Therefore, the top and base of a lithologic unit may be picked with improved accuracy.

Thickness maps were generated for the Brazil and Red Oak Sandstones using the time horizons in the inversion data and average velocity calculated from sonic logs (Figure 33). Cross-plots of seismic thickness between horizons in the inversion data versus well log thickness between tops picked in the logs were created to check the quality of the isochore maps (Figure 34). Trend lines were drawn for the Brazil and Red Oak and yielded poor correlation coefficients of 0.047 and 0.26 respectively. The approximate vertical resolution of the intervals was calculated by dividing the wavelength by 4. The wavelength was calculated by dividing the average velocity calculated from the sonic log data, by the peak frequency from the power spectrum. Using a velocity of 11,827.428 ft/s and a peak frequency of 31.275 Hz, the resolution thickness of the intervals was determined to be approximately 95 feet. The well log thicknesses range from 60-130 feet in the Red Oak Sandstone, and 30-140 feet in the Brazil Sandstone showing the thickness variation in the two sandstones due to their depositional environment.

The seismic thicknesses range from 80-130 feet in the Red Oak Sandstone, and 70-100 feet in the Brazil Sandstone. Portions of both units are thinner than the seismic resolution, and will not be resolved by the seismic reflection data. The poor correlation between the seismic thickness and well log thickness is due to the wide range of velocities that exist in each interval due to the heterogeneous nature of the units (Figure 31). Because the average velocity of the interval includes values from shale (slow) and from sandstone (faster), the resulting velocity yields poor thickness values (Figure 34). The correlation between the actual well thickness and predicted seismic thickness is too poor to derive thickness information from the seismic.

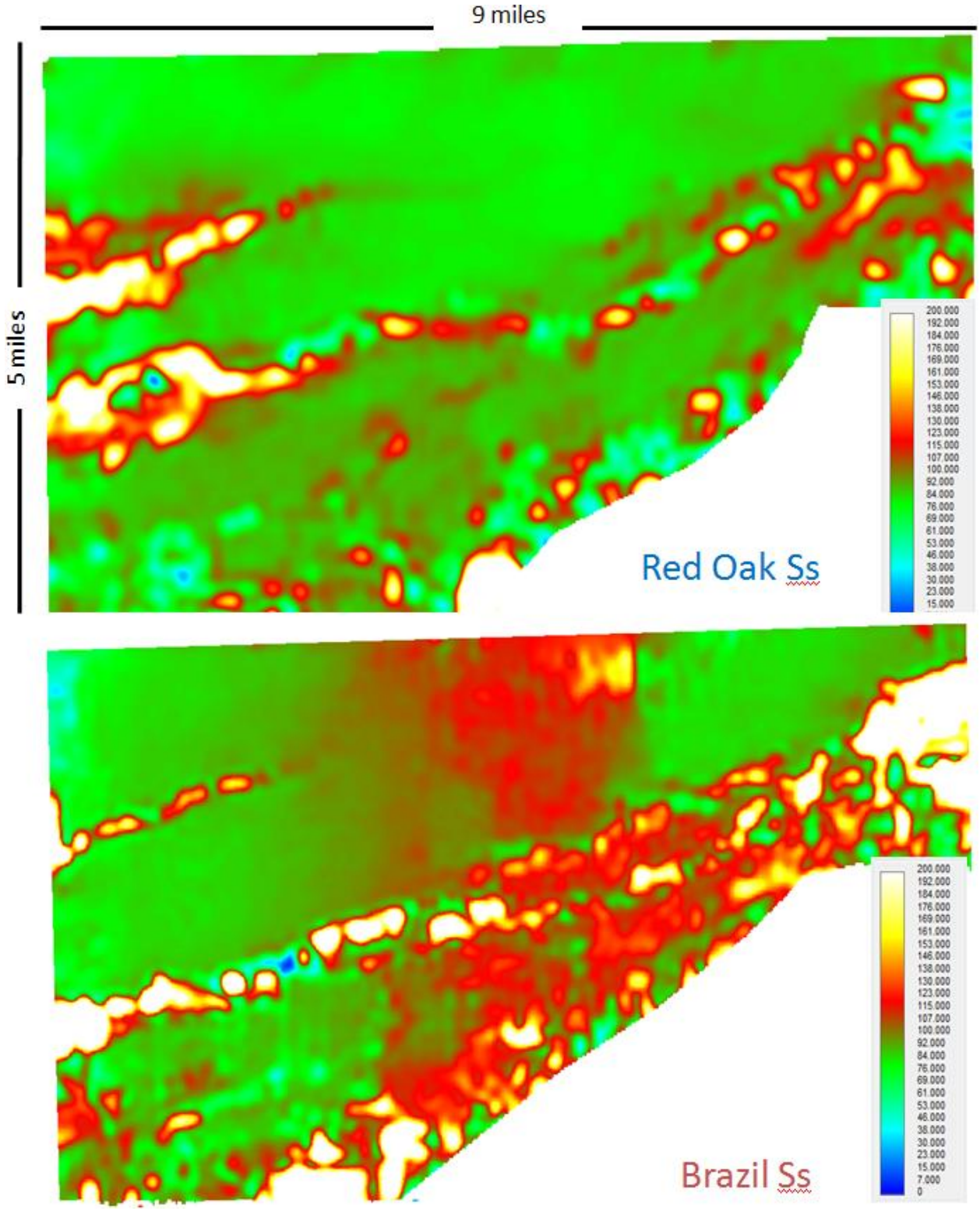

Figure 33. Isochron maps of the Brazil and Red Oak Sandstones. Cooler colors (blues and greens) represent thinner areas and warmer colors (reds and yellows) represent thicker areas. Color bar is in feet. SS=Sandstone

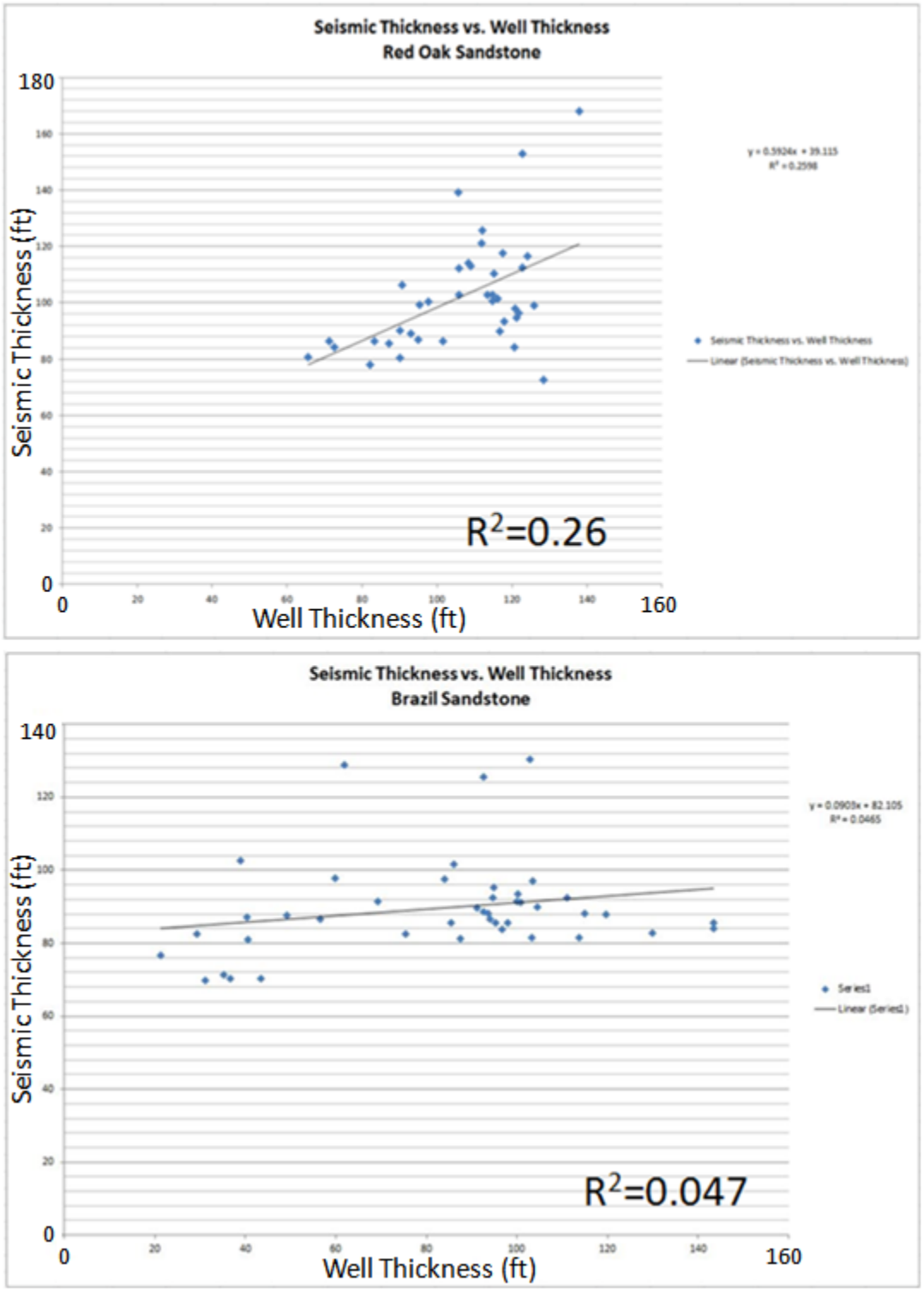

Figure 34. Seismic thickness (from isochore map) versus well log thickness from the top to base of each interval.

CHAPTER 7

CONCLUSIONS

The findings of this thesis are broken into three different categories based on their relationship to acoustic impedance in the Brazil and Red Oak Sandstones: structure, porosity, and thickness.

Porosity:

- A linear correlation between calculated acoustic impedance and porosity in the sandstone portions of the Red Oak and Brazil rock units exists. Higher porosities correlated to areas of lower acoustic impedance within the sandstone portions of the units.
- Interbedded shale within these units inhibits a reliable correlation between the seismic acoustic impedance and porosity.
- To predict reservoir quality of conventional reservoirs, this method should be limited to homogenous sandstones.

Structure:

- The absolute value of acoustic impedance was unaffected by nearby faults. Overall, the strata are mildly deformed and structure had no effect on the acoustic impedance values.
- Using seismic inversion data solely, as a tool for predicting fracture concentration and stress direction orientation does not work. Core data or formation imaging logs (FMI) are needed to verify the existence of open fractures where lower acoustic impedance values occur around faults in the inversion data.

Thickness:

- Isochore maps were generated from the inversion data to predict thickness changes in the Brazil and Red Oak Sandstones. These maps were checked with well log thickness and showed a poor correlation of 0.047 for the Brazil and 0.260 for the Red Oak due to velocity variation in the units. Therefore, seismic thickness cannot be used to predict actual thickness.

REFERENCES

Al-Moqbel, A.M., 2002, Reservoir characterization using seismic reflectivity and attributes: Cambridge, Massachusetts Institute of Technology, M.S. thesis, 82 p.

Arbenz, J.K., 1989, Ouachita thrust belt and Arkoma basin, *in* R.D. Hatcher, Jr., W.A. Thomas, and G.W. Viele, eds., The Appalachian-Ouachita orogen in the United States: GSA, Geology of North America, v. F-2, p.621-634.

Banihasan, N., M.A. Riahi, and H.M. Anbaran, 2006, Recursive and sparse spike inversion methods on reflection seismic data, Institute of Geophysics, University of Tehran.

Berry, R.M., and W.D. Trumbley, 1968, Wilburton gas field, Arkoma basin, Oklahoma, *in* L.M. Cline, ed., A guidebook of the western Arkoma basin and Ouachita Mountains: OCGS Guidebook, p. 86-103.

Blakey, R.C., 2005, Paleogeography and Geologic Evolution of North America, http://www4.nau.edu/geology/.

Branan, C.B., Jr., 1968, Natural gas in Arkoma basin of Oklahoma and Arkansas, *in* B.W. Beebe and B.F. Curtis, eds., Natural gases of North America, v. 2: AAPG Memoir 9, p. 1616-1635.

Calderon, J.E., and J. Castagna, 2007, Porosity and lithologic estimation using rock physics and multi-attribute transforms in Balcon field, Colombia: The Leading Edge, v. 26, p. 142-150.

Castagna, J., 2007, Nautilus USA course notes, Seismic attributes for exploration and reservoir characterization.

Çemen, I., Z. Al-Shaieb, F. Hess, S. Akthar, and R. Feller, 1995, Geometry of thrusting in the Wilburton gas field and surrounding areas, Arkoma basin, Oklahoma: Implications for gas exploration in the Spiro sandstone reservoirs, AAPG Abstracts, p. 84.

Çemen, I., A. Sagnak, and S. Akthar, 2001, Geometry of the triangle zone and duplex structure in the Wilburton gas field area of the Arkoma basin, southeastern Oklahoma, *in* K.S. Johnson, ed., Pennsylvanian and Permian geology and petroleum in the southern Midcontinent, 1998 symposium: OGS Circular 104, p. 87-98.

Çemen, I., J. Evans, and A. Sagnak, 2001, Eastern continuation of the Wilburton triangle zone in the Red Oak gas field area, frontal Ouachitas-Arkoma basin transition zone, southeastern Oklahoma, *in* K.S. Johnson, and D.F. Merriam, eds., Petroleum systems of sedimentary basins in the southern midcontinent, 2000 symposium: OGS Circular 106, p. 81-95.

DeCelles, P.G., and K.A. Giles, 1996, Foreland basin systems: Basin Research, v. 8, no. 2, p. 105–123.

Francis, A., 2006, Nautilus USA course notes, A practical guide to inversion and stochastic modeling, Earthworks Environment and Resources Ltd.

Garcia, G., 2012, Schlumberger, Personal Communication.

Gross, J.S., S.A. Thompson, B.L. Claxton, and M.B. Carr, 1995, Reservoir distribution and exploration potential of the Spiro sandstone in the Choctaw trend, Arkoma basin, Oklahoma and Arkansas: AAPG Bulletin, v. 79, no. 2, p. 159-185.

Hager, C.R., 2009, Seismic interpretation of the Pennsylvanian Atokan strata using 3D seismic inversion data in the Wilburton gas field, Arkoma basin, southeastern Oklahoma: Stillwater, Oklahoma State University, M.S. thesis, 99 p.

Ham, W.E., 1978, Regional geology of the Arbuckle mountains, Oklahoma: OGS Special Pubication 73-3, p. 61.

Hampson and Russell Software Services Ltd., 1999, STRATA.

Houseknecht, D.W., 1986, Evolution from passive margin to foreland basin: the Atoka Formation of the Arkoma basin, south-central U.S.A., *in* P.A. Allen and P. Homewood, eds., Foreland basins: Boston, Blackwell Scientific Publications, International Association of Sedimentologists, Special Publication 8, p. 327-345.

Houseknecht, D.W., and J.A. Kacena, 1983, Tectonic-sedimentary evolution of the Arkoma basin: SEPM, Mid-Continent Section, v. 1, p. 3-33.

Houseknecht, D.W., and T.A. McGilvery, 1990, Red Oak field, *in* E.A. Beaumont and N.H. Foster, compilers, Structural traps II. Traps associated with tectonic faulting:AAPG Treatise of Petroleum Geology Atlas of Oil and Gas Fields, p. 201-225.

Johnson, K.S., ed., 1988, Shelf-to basin geology and resources of Pennsylvanian strata in the Arkoma basin and frontal Ouachita Mountains of Oklahoma: OGS Guidebook 25, 105 p.

Leiceaga, G.G., S.A. Berhanu, A.J. Vargas, J. Silva, L. Zhang, D. Ng, and C. Sanz, 2011, A seismic reservoir characterization work flow for reducing risk utilizing AVO, simultaneous prestack inversion, and rock physics, *in* K.J. Marfurt, D. Gao, A. Barnes, S. Chopra, A. Corrao, B. Hart, H. James, J. Pacht, and N.C. Rosen, eds., Attributes: new

views on seismic imaging-their use in exploration and production, 2011 symposium: GCSEPM, p. 721-749.

McGilvery, T.A., and D.W. Houseknecht, 2000, Depositional systems and diagenesis of slope and basin facies, Atoka Formation, Arkoma basin, *in* K.S. Johnson, ed., Marine clastics in the southern Midcontinent, 1997 symposium: OGS Circular 103, p. 129-140.

Mehdi, S.Y., 1997, Structural geometry of thrust systems in the Red Oak and Talihina Quadrangles, Latimer and Leflore Counties, Arkoma basin, southeastern Oklahoma: Stillwater, Oklahoma State University, M.S. thesis, 113 p.

Morris, R.C., 1974, Sedimentary and tectonic history of the Ouachita mountains, *in* W.R. Dickinson, ed., Tectonics and sedimentation: SEPM Special Publication 22, p. 120-142.

Nicholas, R.L., and D.E. Waddell, 1982, New Paleozoic subsurface data from the north-central Gulf Coast, GSA Abstract with Programs, no. 14, p. 576.

Parker, W.F., Jr., 2007, Structural interpretation of Paleozoic strata as part of the transition zone in the Wilburton gas field using 3D seismic, Hartshorne, Higgins, Adamson, and Gowen Quadrangles, southeastern Oklahoma, Arkoma basin: Stillwater, Oklahoma State University, M.S. thesis, 82 p.

Pedersen-Tatalovic, R., A. Uldall, N.L. Jacobsen, T.M. Hansen, and K. Mosegaard, 2008, Event based low frequency impedance modeling using well logs and seismic attributes: The Leading Edge, vol. 27, p. 592-603.

Pendrel, J., 2001, Seismic inversion- the best tool for reservoir characterization: CSEG Recorder, p. 5-12.

Robinson, E.A., and M.T. Silva, 1978, Digital signal processing and time series analysis, Holden-Day, Inc.

Robinson, D.M., R.M. Bailey, and A.M. Goodliffe, 2012, Structure of the Alleghanian thrust belt under the Gulf Coast plain of Alabama: GCAGS Journal, vol. 1, p. 44-54.

Ronck, J.L., 1997, Structural geology of thrust faulting in the Wister Lake area of the frontal Ouachita mountains, Arkoma basin, southeastern Oklahoma: Stillwater, Oklahoma State University, M.S. thesis, 115 p.

Sadeqi, A.W., 2007, Structural geometry of the Late Paleozoic thrusting in the Hartshorne, Higgins, Adamson, and Gowen Quadrangles, southeastern Oklahoma: Stillwater, Oklahoma State University, M.S. thesis, 89 p.

Schlumberger Limited, 2009, http://www.slb.com/

Suneson, N.H., 2012, Arkoma basin petroleum-past, present, and future, a geologic journey through the Wichitas, Black Mesa basalt, and much more: Shale Shaker, v.63, no. 1, p. 38-70.

Sutherland, P.K., 1988, Late Mississippian and Pennsylvanian depositional history in the Arkoma basin area, Oklahoma and Arkansas: GSA Bulletin, v. 100, no. 11, p. 1787-1802.

Visher, G.S., and S.G. Vedros, 1978, The Red Oak sandstone: a hydrocarbon-producing submarine fan deposit, *in* D.J. Stanley and G. Kelling, eds., Sedimentation in submarine canyons, fans, and trenches: Struidburg, Pennsylvania, Dowden, Hutchinson and Ross, p. 292-308.